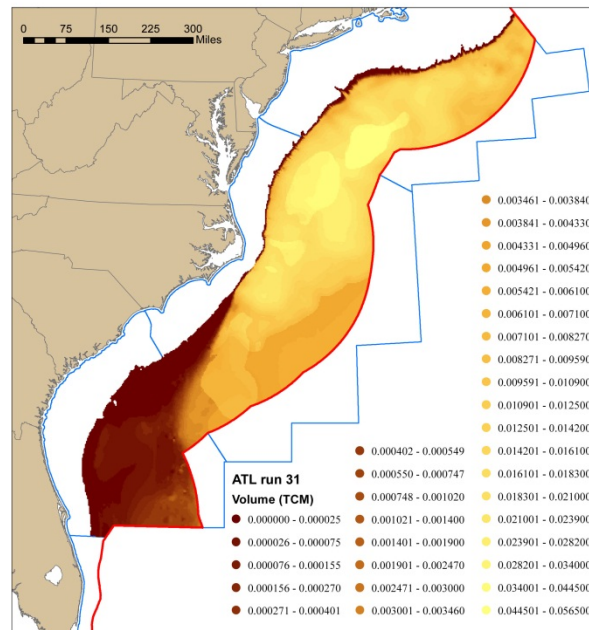


Gas Hydrate Resource Assessment

Atlantic Outer Continental Shelf

BOEM Report RED 2013-01



U.S. Department of the Interior
Bureau of Ocean Energy Management
Resource Evaluation Division
June 1, 2013



Front Cover Image. *Map view of the mean in-place gas hydrate volume. Units are trillion cubic meters ($1 \times 10^{12} \text{ m}^3$) of methane per 9 km^2 model cell expressed at surface temperature and pressure.*

Gas Hydrate Resource Assessment

Atlantic Outer Continental Shelf

SPATIAL ANALYSIS OF INPUTS & OUTPUTS

+

GRAPHICAL & MATHEMATICAL DESCRIPTION OF MODELS AND SUB-MODELS

Model version 5.56

By

Matthew Frye

William Shedd

Jack Schuenemeyer



Acknowledgements

Many of the concepts and methodologies described in this report were transferred or adapted from the workflow described in [OCS Report MMS 2008-004](#). Thus, we recognize those individuals that were instrumental in the development of the original BOEM gas hydrate assessment model workflow or contributed data to that project: Tim Collett, Rick Colwell, Richard Desselles, Barry Dickerson, Scott Edwards, Dick Fillon, John Grace, Jeff Hanor, Jess Hunt, Gordon Kaufman, Gary Lore, Charlie Paull, Pulak Ray, Carolyn Ruppel, Roger Sassen, and Dendy Sloan.

Ray Faith was responsible for the programming of this model.

Helpful reviews of this report were provided by Ray Boswell, Tim Collett, Carolyn Ruppel, and Keith Meekins.

While the many contributions to this project are gratefully recognized, the authors alone accept responsibility for the content of this report.

Any use of trade name, product, or professional services is for descriptive purposes only and does not imply endorsement by the U.S. Government.

Contents

1.0 INTRODUCTION	1
1.1 Atlantic Outer Continental Shelf Gas Hydrate Assessment Model	1
1.2 Areas Assessed	1
1.3 Geologic Setting	1
1.4 Results Summary	2
2.0 MODEL OVERVIEW	3
2.1 Data Available	3
2.2 Model Parameters	4
3.0 ATLANTIC – GOM MODEL DIFFERENCES	4
4.0 SPATIAL INPUTS	5
4.1 Water Depth	5
4.2 Sediment Thickness	6
4.3 Sand Percent	6
4.4 Bottom Simulating Reflectors	7
5.0 SPATIAL OUTPUTS	7
5.1 Charge Module	7
5.2 Container Module	10
5.3 Concentration Module	10
5.4 Integration Module	10
6.0 CELL DEPENDENCY	11
7.0 GRAPHICAL AND MATHEMATICAL MODEL COMPONENTS	11
7.1 Charge Module	12
7.1.1 Generation Model	12
7.1.1.1 Sub-model: Total Organic Carbon (TOC)	12
7.1.1.2 Sub-model: Methanogenic Production Function	13
7.1.1.2.1 Maximum Initial Production	14
7.1.1.2.2 Sub-model: Permeability	14

7.1.1.2.2.1 Permeability at Water Bottom (WBP)	15
7.1.1.2.2.2 Sand Permeability as a Function of Depth	15
7.1.1.2.2.3 Shale Permeability as a Function of Depth	15
7.1.1.2.2.4 Average Rock Bulk (Midpoint) Permeability	17
7.1.1.2.3 Sub-model: Sediment Temperature	17
7.1.1.2.3.1 Water Bottom Temperature	17
7.1.1.2.3.2 Sediment Temperature	17
7.1.1.2.4 Sub-model: Asymptotic Conversion Efficiency	18
7.1.1.3 Allocation of Sediment Thickness to Deposition by Geologic Time	18
7.1.1.4 Generation Potential (GP)	19
7.1.1.5 Incremental Generation (IG)	19
7.1.1.6 Resultant Generation	20
7.1.2 Migration Model	20
7.2 Container Module	21
7.2.1 Gross Hydrate Stability Zone Thickness Model	21
7.2.1.1 Geothermal Gradient (GTG)	23
7.2.1.2 Phase Stability Submodel	23
7.2.2 Undersaturated Zone Thickness Model	25
7.2.3 Net Hydrate Stability Zone Thickness Model	25
7.3 Concentration Module	25
7.3.1 Porosity from shallow sand (SSP)	25
7.3.2 Porosity from shallow shale (SHP)	26
7.3.3 Methane Saturation of Volume of Total Void Space	27
7.3.3.1 Hydrate saturation in sand (SatS)	27
7.3.3.2 Hydrate saturation in shale (GHS)	27
7.3.4 Total Saturated Void Space	28
7.4 Integration Module	28
7.4.1 Volume Computation	28

7.4.2 Formation volume factor (fvf) – volume at the surface	29
8.0 RESULTS	29
8.1 Sand Reservoirs	31
8.2 Model Calibration	33
8.3 Previous Resource Estimates	33
8.4 Disclaimer	33
9.0 REFERENCES	34
Appendix A - Atlantic setup parameter file run R31	36
Appendix B - Geothermal gradient workflow	37
Appendix C - Shallow shale porosity model	46
Appendix D - Case Study: Blake Ridge area near ODP wells 994, 995, and 997	48

This page intentionally left blank

1.0 INTRODUCTION

1.1 Atlantic Outer Continental Shelf Gas Hydrate Assessment Model

The Bureau of Ocean Energy Management (BOEM) Atlantic Outer Continental Shelf (OCS) gas hydrate assessment model comprises a spatially resolved, cell-based stochastic model structure that utilizes a mass balance approach to calculate the volume of gas hydrate in place in the subsurface. The assessment model includes three computational modules and an integration module (Figure 1), as well as numerous sub-models that attempt to quantify the many components necessary for a working gas hydrate petroleum system¹. The stochastic model structure allows for the introduction of component uncertainties at many levels throughout the model, resulting in a probabilistic distribution of results. Geologic risk is not introduced at any level in the model.

The Atlantic gas hydrate model employs the same general approach and comprises the same four computational modules that are used in the 2008 Gulf of Mexico (GOM) gas hydrate assessment and reported on extensively in [OCS Report MMS 2008-004](#). Changes to the 2008 GOM model that allow adaptation to the Atlantic OCS are described in Section 3.0 of this report (p. 4).

It is important to note that the values reported here are reflective of *in-place* volumes of gas hydrate reported at standard temperature and pressure. References to technically recoverable gas hydrate resources are absent from this report, as production technologies are in their infancy and sustained commercial production from gas hydrate reservoirs has not been demonstrated anywhere in the world.

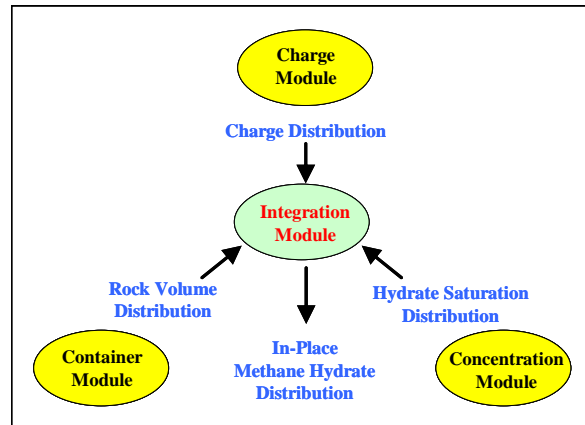


Figure 1. Gas hydrate assessment model structure comprising three process modules and an integration module.

1.2 Areas Assessed

The Atlantic OCS includes the submerged lands from 3 nautical miles (Federal/State boundary) to 200 nautical miles (U.S. Exclusive Economic Zone; EEZ) seaward of the eastern U.S. coastline (Figure 2). The Atlantic OCS is divided into four planning areas (North Atlantic, Mid-Atlantic, South Atlantic, Straits of Florida) that together comprise a total area in excess of 269 million acres (420,000 mi²; 1,089,128 km²)(Figure 2). The Atlantic gas hydrate assessment includes those areas in the North-, South-, and Mid-Atlantic planning areas inside of the U.S. EEZ where water depth is greater than 300 meters (m). Excluded from this assessment is the Straits of Florida planning area due to a paucity of subsurface data and a perceived lack of gas hydrate resource potential.

1.3 Geologic Setting

The present day Atlantic OCS consists of a tectonically passive margin underlain by Jurassic and younger sedimentary rock. A pronounced shelf/slope break that coincides with a buried Mesozoic shelf edge reef complex, where water depths quickly increase from < 200 m to greater than 4,000 m, is present along the entire margin. The shallow continental shelf is much broader in the South Atlantic planning area than in the Mid- and North Atlantic margin. Locally thick depocenters and sedimentary basins proximal to the present day coastline contain greater than 5,000 m of sediment in many places.

¹ In addition to typical petroleum system elements, such as gas charge and reservoir, an analysis of the gas hydrate petroleum system requires that the unique thermodynamic conditions that enable hydrate formation be modeled.

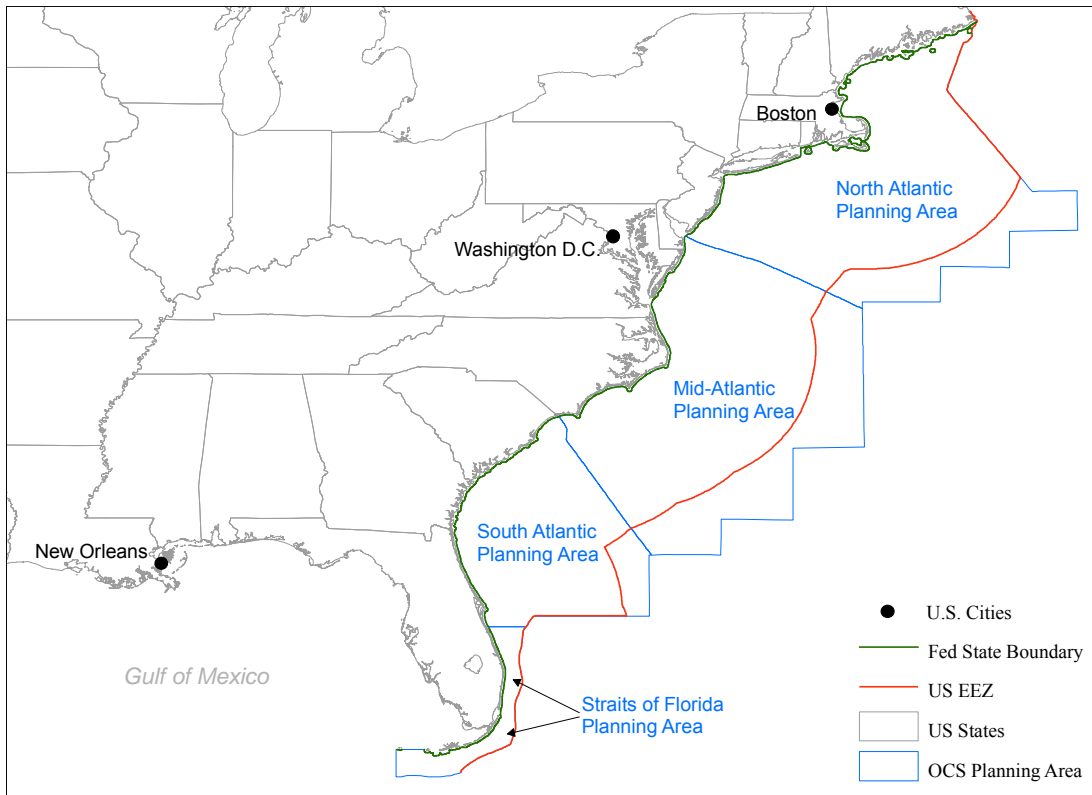


Figure 2. Map of eastern United States and the Atlantic Outer Continental Shelf (OCS). Only the North, Mid-, and South Atlantic Planning Areas are included in this study.

Recent sedimentation (Pleistocene and younger; < 1.95 million years) has been focused on the Mid- and North Atlantic margin in an area outboard of the modern shelf/slope break. Thick wedges of Pleistocene sediment (> 2 km) are located on the mid- to lower rise in an area characterized by large incised canyons at the shelf edge (Hudson Canyon, Baltimore Canyon). In general terms, the north Atlantic margin has been recently subject to a much greater influx of terrigenous sand and silt-sized sediment than the south Atlantic.

1.4 Results Summary

Undiscovered gas hydrate resources on the Atlantic OCS from this assessment are shown in Table 1, where the Mean value is the expected value, and the P95 and P5 values indicate that there is a 95% and 5% probability, respectively, that gas hydrate resources of at least these quantities exist.

Region Planning Area	In-Place Gas Hydrate Resources					
	Trillion Cubic Feet (Tcfg)			Trillion Cubic Meters (Tcmg)		
	P95	Mean	P5	P95	Mean	P5
Atlantic OCS	2056	21702	52401	58	614	1483
North Atlantic PA		8433.28			238.81	
Mid-Atlantic PA		13115.85			371.40	
South Atlantic PA		152.73			4.32	

Table 1. Gas hydrate resources on the Atlantic OCS.

2.0 MODEL OVERVIEW

The modeling approach employed by BOEM for the assessment of in-place gas hydrate on the OCS is different than that used to assess undiscovered conventional oil and gas resources. Whereas most conventional oil and gas assessments utilize information derived from discovered oil and gas pools in a given play to predict the undiscovered resource potential remaining in that play (e.g. Dunkel and Piper, 1997), the gas hydrate assessment methodology for deep marine settings on the OCS must allow for the paucity of actual field-size information. Thus, here we employ a stochastic mass balance model that includes the three computational modules and a single *Integration* module shown in Figure 1. For every model cell at every trial run, Monte Carlo sampling of uncertain modeling variables generate a value for the thickness of the hydrate stability zone (HSZ; the *Container* module); a value that represents the fraction of the HSZ that can be saturated with gas hydrate (the *Concentration* module); and a value for the amount of biogenic gas available to charge the HSZ (the *Charge* module). The volume of gas available is compared to the container space available in the *Integration* module, and the smaller of the two volumes is recorded. While the desired end product of an assessment model run is an in-place volume of gas hydrate (reported as the volume of methane at surface temperature and pressure), any of the interim calculations and results (such as those of the computational modules) can be reported in either graphical or spatial expressions.

2.1 Data Available

All of the spatially-recognized model inputs (described in Section 4) and many of the empirically-based data sets (Section 7) are derived from geological and geophysical data acquired on the Atlantic OCS. Spatially referenced input files were enabled through project access to over 200,000 line miles (~320,000 line km) of 2-D multi-channel seismic data (Figure 3).

Fifty one permitted wells have been drilled in the Atlantic OCS, including five stratigraphic test wells drilled between 1975 and 1979 and 46 industry wells drilled between 1977 and 1984. These wells are tightly grouped within three sedimentary basins (Southeast Georgia Embayment, Baltimore Canyon Trough, and Georges Bank Basin; Figure 4) that contained promising commercial oil and gas targets at the time that they were drilled. All of the industry wells are permanently plugged and abandoned, and none has achieved sustained production of oil or natural gas.

Scientific wellbores drilled by the Deep Sea Drilling Program (DSDP) and its successor Ocean Drilling Program (ODP) provide a significant source of subsurface geologic data on the Atlantic OCS. For this assessment, summary reporting on over fifty DSDP/ODP wells (Figure 4) was examined and provided critical information on subsurface conditions, such as local organic geochemistry, lithostratigraphy, and thermal gradients.

Information from ODP Leg 164 wells at Sites 994, 995, and 997 proved exceptionally valuable to this

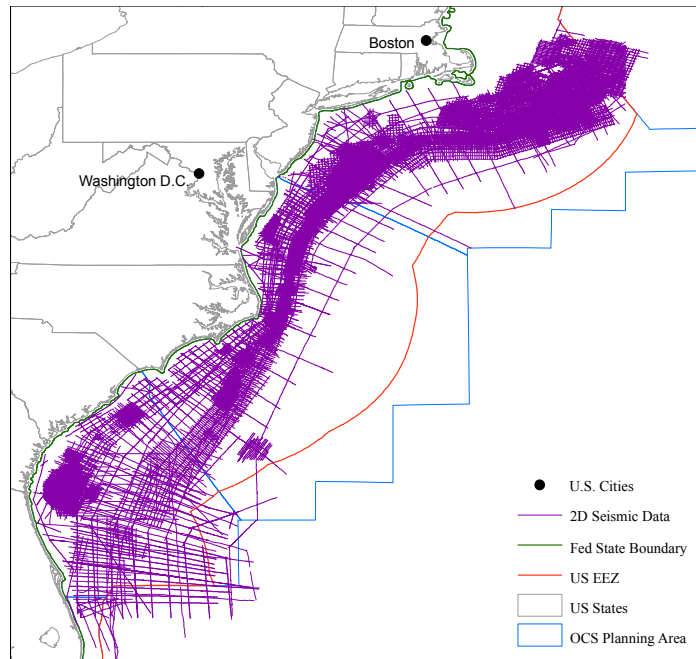


Figure 3. Location map of 2-D seismic data on the Atlantic OCS. No 3-D seismic data were available for this assessment.

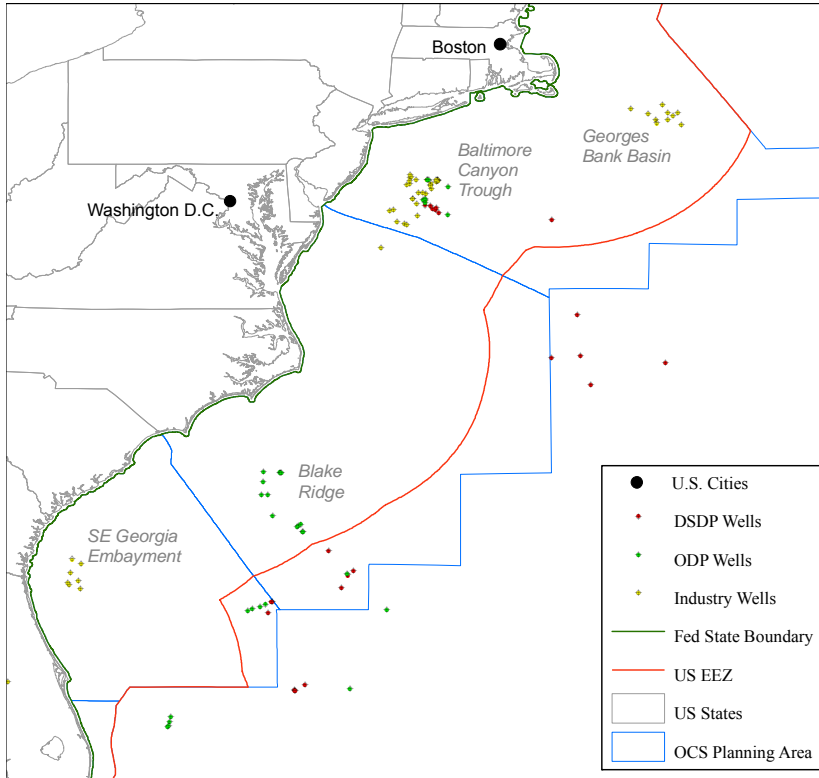


Figure 4. Location map of well data used in the project. Note the asymmetry of distribution of wells across the OCS, particularly the industry wells (grouped into the SE Georgia Embayment, the Baltimore Canyon Trough, and the Georges Bank Basin). Also note the focused approach of scientific wells on the Blake Ridge gas hydrate province.

assessment, as these wells targeted a large gas hydrate accumulation on the Blake Outer Ridge in the Mid-Atlantic planning area (e.g. Paull et al., 2000; Figure 4). Site characterization and volumetric resource estimates at these locations (e.g. Collett and Ladd, 2000) provide critical calibration points for the BOEM assessment model.

2.2 Model Parameters

For the purpose of this assessment, the Atlantic OCS has been partitioned into 57,066 cells of size 3 km x 3 km, with a total study area measuring approximately 514,000 km². The assessment model input file comprises a data table where each model cell is recognized by paired XY coordinates and is assigned a unique attribute from each of the spatial inputs described in the next Section. Calculated model throughputs and outputs are mapped back to the same geographic location.

The model itself is programmed in FORTRAN code and is run for 1,000 trials. Sensitivity analysis of the results indicates that 1,000 trials yields stable estimates of means and reasonably stable estimates of the 5th and 95th percentiles. Additional runs up to 4,000 trials can be executed, and model parameters may be changed by the user at run time. Any changes in the functional form of a model would need to be incorporated in the FORTRAN code and the resultant code recompiled.

An example of the Setup Excel file containing local model parameters is shown in Appendix A.

3.0 ATLANTIC – GOM MODEL DIFFERENCES

Subsequent to the release of the 2008 GOM model and accompanying methodology report, a number of changes have been made to the functional form of the model. Changes to the Atlantic model include the exclusion of lateral dip-driven gas migration; estimation of under-saturated zone thickness rather than an inverse relationship to charge; the exclusion of seafloor seismic anomalies as a model component; the inclusion of seismic bottom simulating reflectors (BSR) as a proxy for migration efficiency; and, the

estimation of sediment thickness (from two chronologic units) based on subsurface mapping, and the subdivision of one of those units by equal intervals. Table 2 provides a concise summary of the changes. Finally, empirical distributions of many input parameters, such as geothermal gradient (GTG), total organic carbon (TOC), and water bottom temperature (WBT) were changed based on the inclusion of local data sources.

Module	Model	Atlantic Model	Gulf of Mexico Model
Charge	Sediment Thickness	Spatial input (ISO 1 and ISO 2)	Estimated from gamma distributions
Charge	Migration	100% vertical	Combination of vertical & dip driven
Charge	Migration Efficiency	Function of BSR	Randon draw from beta(4, 10) distribution
Container	Undersaturated Zone	Symmetric beta (0 to 400 m)	Inversely proportional to charge (0 to 200 m)
<i>Input</i>	Surficial Anomaly	Not Modeled	Presence changes gas composition used in Container module and adds fracture saturation to Concentration module
<i>Input</i>	Salt	Not Modeled ¹	Subseafloor depth to salt influences HSZ thickness
<i>Input</i>	BSR	Used for Migration Efficiency	Not Modeled ²

The following inputs were developed for the Atlantic based on local information, and may comprise a different functional form than the same inputs in the GOM: GTG, WBT, TOC, Quality

¹While shallow salt has not been included in the Atlantic assessment model, it is noted that a ssw/nne trend of piercement salt features of limited areal extent is recognized near the Carolina Trough.

²BSRs were not included in the original GOM model; BOEM now has identified over 140 BSRs in the GOM (Shedd et al, 2011).

Table 2. Summary of recent changes to the BOEM model.

4.0 SPATIAL INPUTS

The foundation of the in-place gas hydrate assessment in the Atlantic rests on four spatially-resolved input data sets that are derived from the interpretation of 2-D multichannel seismic data and Atlantic wellbore data. In this Section, we describe how the four spatial input datasets were developed², and how they are applied to the Atlantic assessment model structure. The value of each variable within a model cell is represented spatially as a point in the center of the cell.

4.1 Water Depth (Figure 5) is derived from ETOPO1 1 Arc-Minute Global Relief Model, available publicly from the National Geophysical Data Center³. Those areas with water depths less than 300 meters were excluded from the assessment model as they do not support the formation of gas hydrate. Maximum water depths on the Atlantic OCS used as model input did not exceed 5,400 meters. Water depth drives two key variables in the model:

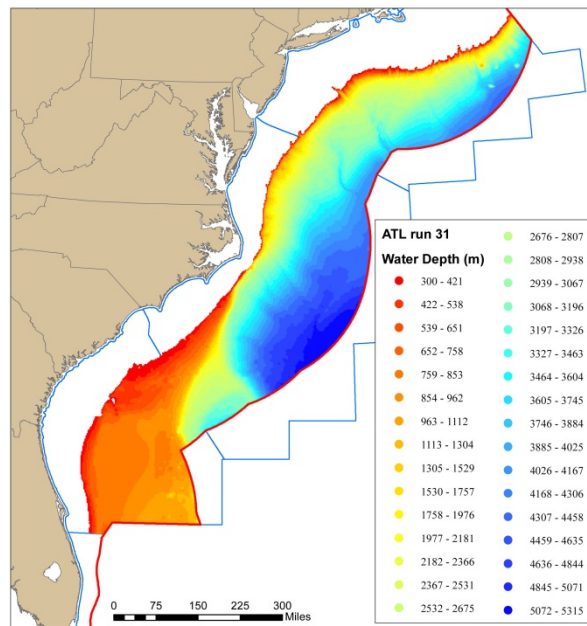


Figure 5. Water depth spatial input map. Depth in meters

² Note that the distribution of seismic and well data is not uniform across the Atlantic OCS (Figures 3 and 4), and interpretive products derived from these data introduce uncertainties that have not been quantified.

³ <http://www.ngdc.noaa.gov/mgg/global/relief/ETOPO1/docs/ETOPO1.pdf>

- Pressures at and below the seafloor, both functions of the hydrostatic pressure of the water column, are determinants of the thickness of the gross HSZ, as calculated in the Container module;
- Temperatures at the seafloor are a function of water depth, and are incorporated with a GTG to predict subsurface temperatures at varying levels below the seafloor. Subsurface temperatures are required to calculate the gross HSZ, and are a critical input in the biogenic gas generation model.

4.2 Two **sediment thickness isopachs** have been generated to define the age and thickness of stratal units that contribute to the Charge module. The upper unit (ISO 1) is bounded by the seafloor and the top of Pliocene horizon. The lower unit (ISO 2) is bounded by the top of Pliocene and the top of Cretaceous. The ISO 1 and ISO 2 surfaces were chosen as map units based on the relative continuity of the seismic reflectors associated with the chronostratigraphic datum. The thickness of these intervals constrains the amount of sedimentary section and total organic carbon that are available to be converted to biogenic gas. The thickness maps of ISO 1 and ISO 2 are shown in Figures 6 and 7, respectively.

4.3 The **percent sand** in the top 2,000 feet (610 m)⁴ of stratigraphic section below the seafloor is interpreted from well log and 2-D seismic data. The areal distribution and vertical concentration of sand and shale volumes in the Atlantic (Figure 8) are important input parameters in both the Charge and Concentration modules of the in-place assessment model. In the Charge module, the relationship between water flux in the source rock and methanogenic productivity is presumed to be direct. We invoke the end member physical properties of sands and shales to model water flux (using permeability as a variable) and apply them through the candidate section using the sand/shale ratio defined here. The sand and shale content of the HSZ is used to define the distribution of porosity and the saturation of available pore space in the Concentration module. It is assumed that the top 2,000 ft of section throughout the study area comprises only sand and shale.

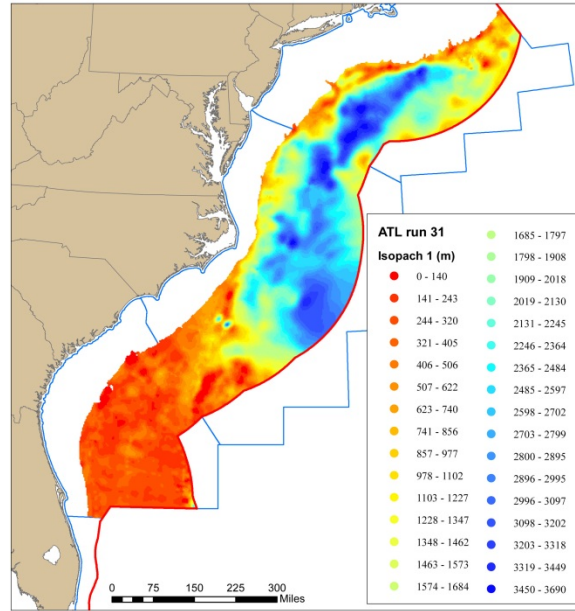


Figure 6. *Isopach 1 spatial input, comprising the section from the seafloor to the top of the Pliocene (approximately 1.95 million years (my)). Thickness in meters.*

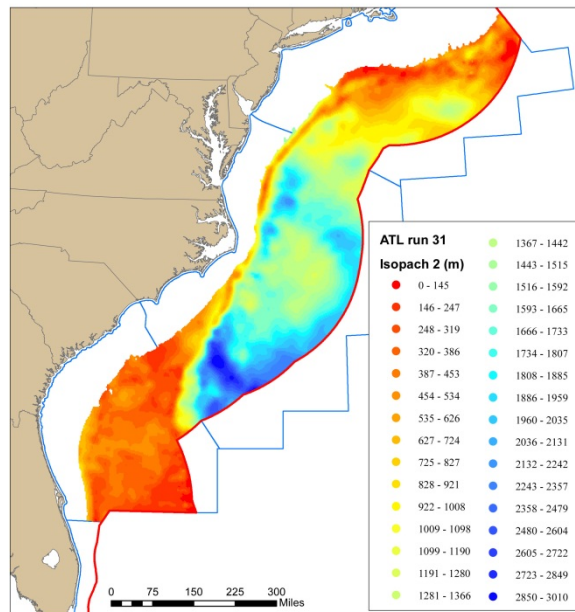


Figure 7. *Isopach 2 spatial input, comprising the section from the top of the Pliocene (1.95 my) to the top of the Cretaceous (65 my). Thickness in meters.*

⁴ We include only the upper 610 m in this analysis as it best reflects the potential sedimentology of the Atlantic OCS hydrate stability zone (Atlantic HSZ mean = 392 m; HSZ max = 597 m).

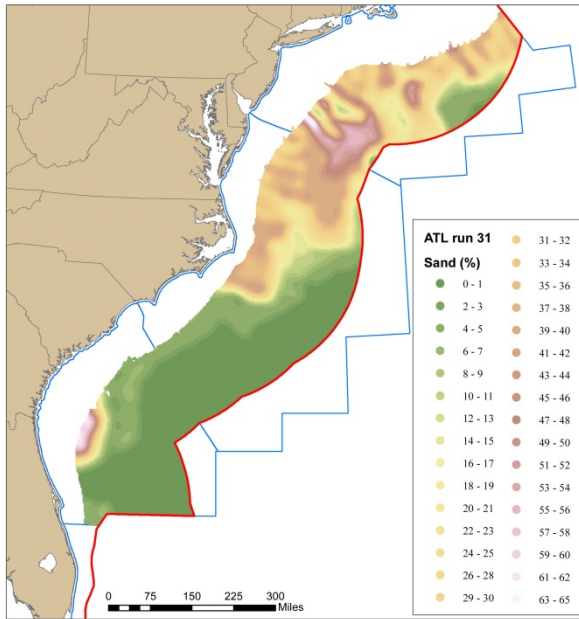


Figure 8. Sand distribution map spatial input, reported as a percent of the upper 2000 ft of stratigraphic section.

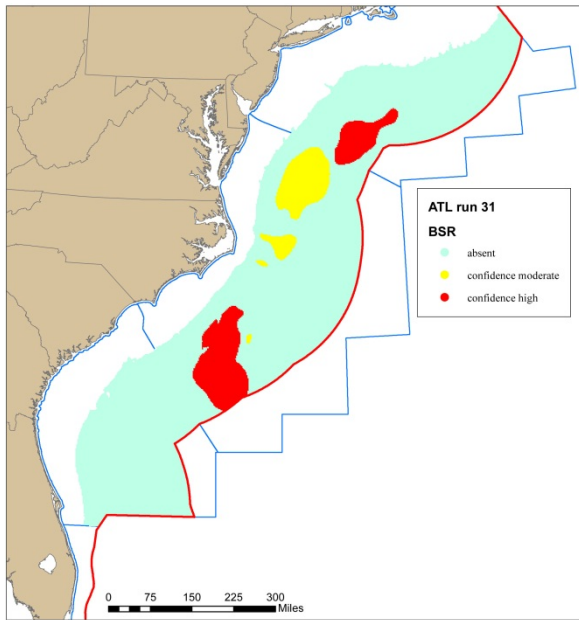


Figure 9. Bottom Simulating Reflector (BSR) distribution spatial input.

4.4 Six unique BSRs were identified from the available 2-D seismic data (Figure 9). BSRs were identified as either “high confidence” or “moderate confidence”. The presence of a high- or moderate confidence BSR, or absence of a BSR, is recorded at each model cell and used to select one of three gas migration efficiency distributions (Section 7.1.2). Model cells in areas of high confidence BSR will be allowed to invoke higher interpreted gas migration efficiencies than those cells where a BSR is absent.

5.0 SPATIAL OUTPUTS

At the end of each trial, cellular model results from the three process modules and the Integration module are recorded. After the user-specified number of trials have been run (1,000 in our case), cell-level results are aggregated and delivered as a nine point empirical distribution. As each model cell is linked to a unique set of lat/long coordinates, any of the nine-point distribution fields can be mapped in a Geographic Information Systems (GIS) environment. For all of the mapped outputs that follow in this report, the *mean* result over all trials is the subject attribute.

5.1 Charge Module

The Charge module comprises two main sub-models: the generation model⁵ and the migration model. The general structure of the biogenic methane generation model is mass balance. In simple terms, a *mass of organic carbon* is input into a *generation productivity function* (Figure 10). This function determines the efficiency of its transformation to biogenic methane and produces an estimate of the output mass of methane. The *time* and *thickness* components shown in Figure 10 are derived from the ISO 1 and ISO 2 spatial input files (Figures 6 and 7), which serve as the primary spatial inputs that drive this model. Typically, a thick sedimentary section (subject to other controls, such as sediment *temperature* and *permeability*) yields a greater mass of produced methane than a thinner sedimentary section. Many of the non-spatial inputs that help drive this transformation are described in detail in Section 7 of this report. The output of the generation model is shown in Figure 11.

⁵ Only biogenic gas is modeled in this assessment. While it is widely recognized that certain source rocks may be locally thermally mature on the Atlantic OCS (e.g. Amato, 1987; Sassen and Post, 2008), we do not have enough source rock information to confidently model the quantity of thermogenic gas that has been generated.

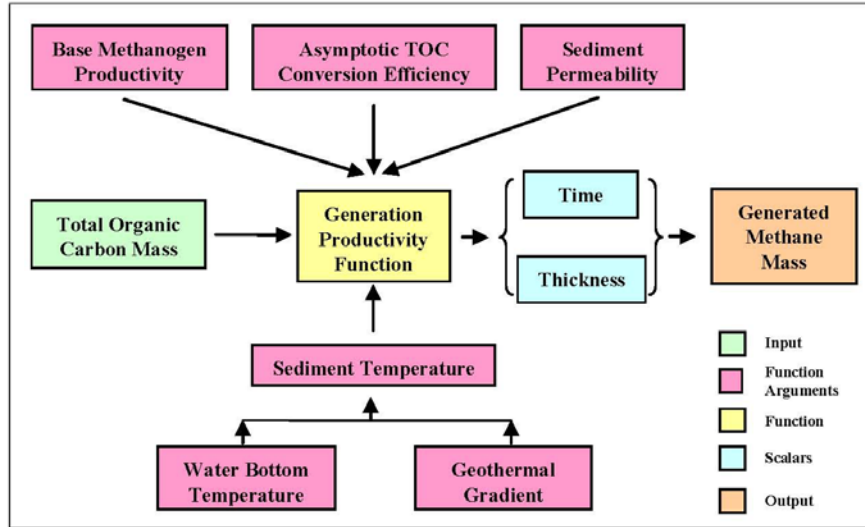


Figure 10. Schematic diagram of the biogenic gas generation model.

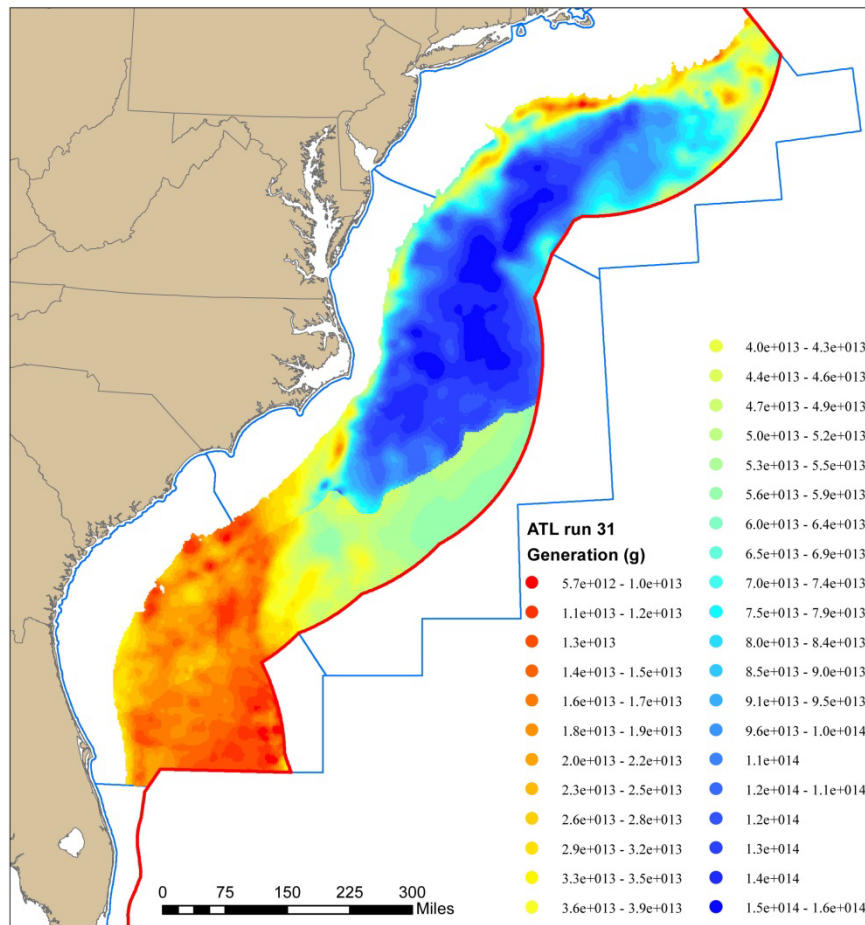


Figure 11. Generation model output (mean value). Note that the highest generation values generally coincide with the areas of thickest sedimentary section. Units are reported as grams of methane per 9 km^2 model cell.

The migration model for the Atlantic OCS has been simplified dramatically from that used in the 2008 GOM model. In simple terms, the complex lateral re-distribution of methane that was employed in the 2008 GOM model has been replaced with a 100% vertical migration model. Two primary reasons justify this change. First, the rugosity of the top of salt surface in the GOM creates a series of mini-basins and intervening salt highs that create natural sub-regional catchment basins and short migration routes; in the Atlantic, this mini-basin architecture does not exist, and dipping surfaces often continue for several tens of miles before an intervening high is reached⁶. In many cases, a shallow subsurface unit in Atlantic abyssal water depths can continue in a singularly updip direction all the way to the outer shelf edge. Second, conventional oil and gas pools and seafloor expulsion features in the GOM align very closely with the intra mini-basin highs, indicating a high degree of focused flow to these areas. This same relationship is not widely observed on the Atlantic margin, likely for many of the same reasons described in the first observation.

The output from the migration model for each model cell in the Atlantic gas hydrate assessment is equal to the generation volume per cell, reduced by some migration efficiency that is calibrated to the presence/absence of a BSR (see Section 7.1.2 for distributions). We refer to the output from this model as the Charge (Figure 12).

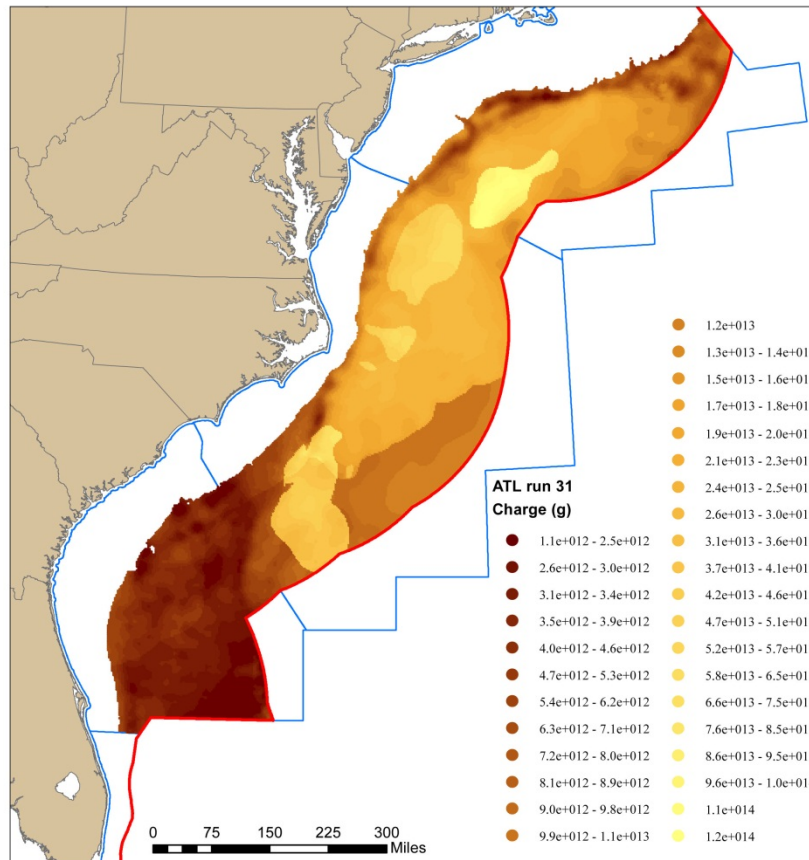


Figure 12. Charge module output mean value (units are reported as grams of methane per 9 km² model cell).

⁶ Our observations from 2-D seismic profiles are in accordance with those made by Tucholke et al. (1977), who observe that certain BSRs on the Atlantic OCS are coincident with structural anticlines and suggest that the relationship invokes a lateral component of gas migration. While we agree with this conceptually, we were unable to introduce a spatial modeling component that accurately captured the re-distribution of gas across the Atlantic OCS.

5.2 Container Module

The mathematical calculation of the HSZ is described in this report in Section 7.2. In general, we employ the same approach that was used in the 2008 GOM model, though small changes were enacted in the Atlantic due to the lack of a widespread shallow salt component. Also, the gas composition in the Atlantic is assumed to be predominantly methane, whereas in the GOM - in areas of seafloor seismic anomaly - we allowed for a gas composition that accommodated heavier hydrocarbons (described in detail later in this report, Section 7.2.1.2).

The container space available to host gas hydrate is calculated through a two-step process. First, a *gross* HSZ is defined by solving the equation shown in Section 7.2 of this report. The mean gross HSZ output (Figure 13) is spatially driven by the bathymetry input. The second step of the Container module removes a layer near the seafloor that is assumed to be undersaturated with respect to methane. Under-saturation is partially due to the presence of sulfate reducing micro-organisms and the downward intrusion of undersaturated sea waters. The remaining thickness of sedimentary section - from the base of the undersaturated zone to the base of the gross HSZ - is referred to as the *net* HSZ. The mean net HSZ thickness is shown in map view in Figure 14. For the purpose of the Atlantic assessment model, the net HSZ is the vertical thickness of the subsurface capable of hosting gas hydrate resources.

5.3 Concentration Module

The Concentration module provides an assessment of the fraction of the net HSZ bulk rock volume capable of hosting gas hydrate. We combine end-member gas hydrate saturation measurements for sand and shale lithologies with modeled subsurface porosities. A compilation of global gas hydrate saturation measurements is presented in Section 7.3.3 of this report. The sand percent spatial input plays an important role in calculation of this value, and its influence can be seen quite clearly when the mean Concentration output map (Figure 15) is compared to the sand percent input (Figure 8).

5.4 Integration Module

The Integration module computes in-place gas hydrate volume by combining results of the three previously described process modules. In simple terms, the charge available to each model cell is compared to the available container space in the gas hydrate stability zone (the product of the Container module and the Concentration module), and the smaller of the two values is retained. This volume is then converted to

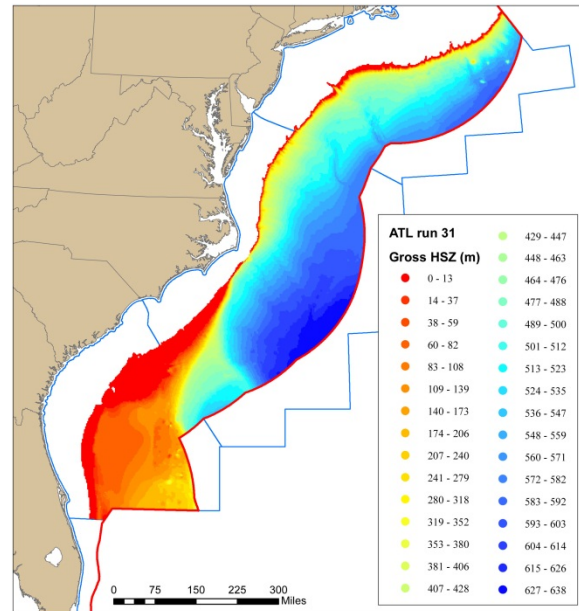


Figure 13. Spatial output of the mean value of the gross HSZ thickness (units = meters).

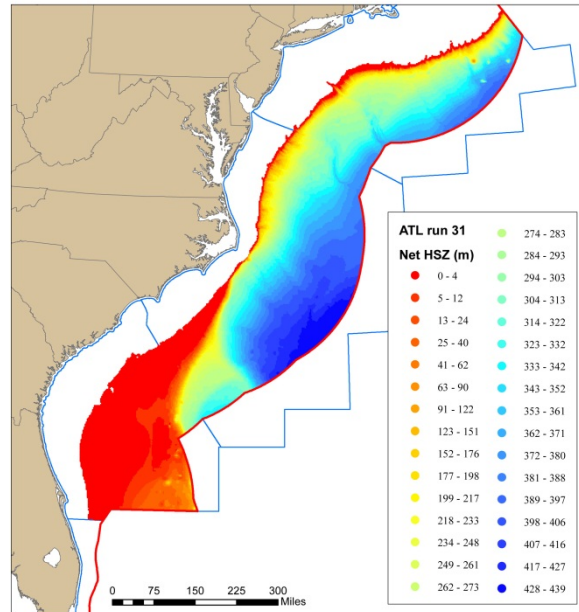


Figure 14. Spatial output of the mean value of the net HSZ thickness (units = meters).

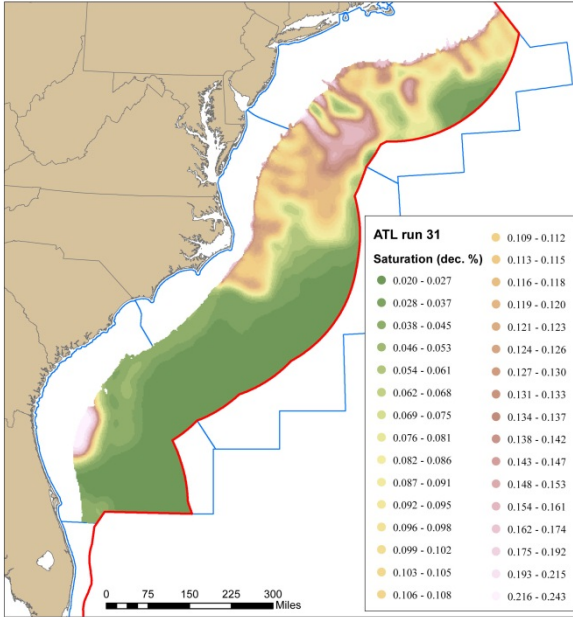


Figure 15. Concentration module mean output, where potential hydrate concentration is expressed as a decimal percent of the bulk rock volume.

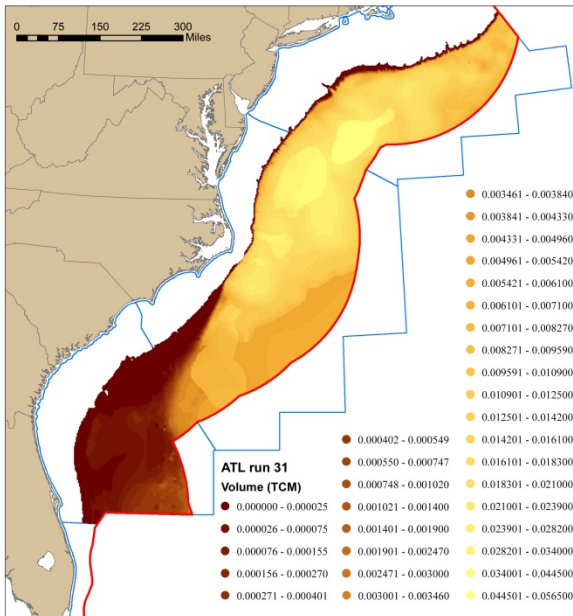


Figure 16. Map view of the mean in-place gas hydrate volume. Units are trillion cubic meters ($1 \times 10^{12} \text{ m}^3$) of methane per 9 km^2 model cell expressed at surface temperature and pressure.

standard temperature/pressure. The mean in-place volume map is shown in Figure 16; units are trillion cubic meters per model cell.

Note that the richest per-cell volumes coincide with areas of BSR, and with those areas that contain relatively thick stratigraphic sections (ISO 1 and ISO 2). The thick stratigraphic sections are capable of providing abundant organically-rich material that can be microbially converted into methane.

6.0 CELL DEPENDENCY

An important issue in assessing the potential of the Atlantic or other large regions is the degree of dependency between model cells. There is recognition that nearby cells may tend to be moderately- to highly-correlated, while those considerably distant from each other are potentially less correlated. Thus, considering individual cells as independent of each other is not appropriate. However, in the Atlantic, the detailed information needed to model possible dependencies by a statistical method does not exist. Instead, two approaches were considered to introduce some manner of spatial correlation. One approach involves the introduction of some partial level of dependency between model cells by considering cells within catchment basins to be dependent. The second modeling approach examined - and the one used for this assessment - was to assume all cells were totally dependent⁷. In this implementation, the same set of random draws used to estimate parameters were used for all cells in a given trial. This approach provides uncertainty interval estimates deemed appropriate for the breadth of knowledge comprising each input of an uncertain quantity.

7.0 GRAPHICAL AND MATHEMATICAL MODEL COMPONENTS

The BOEM gas hydrate assessment model contains four primary Modules (Figure 1), each of which contain some number of models and/or sub-models. At each trial run, the models and sub-models introduce critical input parameters that are derived from data sources *in addition to* the spatially-resolved inputs described in Section 4.

⁷ The modeling approach of cell dependency was also used in the 2008 GOM in-place assessment, although the GOM assessment required the use of four input files (West, Central, East1, and East2) that were subsequently aggregated independently.

Empirically-derived model inputs are drawn from a distribution of data points that come from various geographic locations, but are believed to represent a likely state of nature for any cell in the study area. Examples of these types of input data include the allocation of TOC to a model cell (Section 7.1.1.1) and the assignment of a GTG to a cell (Section 7.2.1.1), among many others.

Calculated model inputs are founded in physical observations and relationships that can be applied across the study area and in many cases are developed as functions of one of the spatially-resolved inputs to the model. For every trial run these values are calculated for each model cell. Examples include the calculation of water bottom temperature as a function of bathymetry (Section 7.1.1.2.3.1) or sediment porosity as a function of burial depth (Section 7.3.1).

All of the empirical distributions and calculation functions that reside in the sub-models can be modified as new or better data are made available. This extreme variable disaggregation allows for the gas hydrate assessment model to be updated easily at any component level. It also allows for the relatively easy adaptation of the model structure to other geologic basins or marine settings in order to capture the influence of local surficial or subsurface conditions.

7.1 Charge Module

The Charge module contains a generation model and a migration model that ultimately calculate the volume of methane gas that is delivered to the HSZ. A single Monte Carlo trial of the generation model produces the amount of biogenic methane produced in each cell at that trial. The migration model then calculates that volume of gas that migrates vertically in the model cell.

7.1.1 Generation Model

In the generation model, a mass of organic carbon is provided to a productivity function that determines the efficiency of its transformation by methanogenic archaea to biogenic methane, and provides an estimate of the output mass (Figure 10). Productivity is defined as a *rate*, measured in grams of methane produced per gram of organic carbon input to the system per unit of time (here per one million years). This process is complex; the model represents the metabolic reactions of communities of methanogenic archaea to changes in their environments as sediments are deposited on the seafloor and progressively buried. The components of Figure 10 are described below.

7.1.1.1 Sub-model: Total Organic Carbon (TOC)

Total organic carbon (TOC) is a significant driver of the generation model. The endowment of TOC is introduced to the model as a weight percent value and scaled up to a mass of organic carbon for each of the six geologic time intervals using a bulk sediment density. The six time intervals include the ISO 1 input thickness and the ISO 2 input thickness divided equally into five units (Section 7.1.1.3). Weight percent TOC data was compiled from borehole data on the Atlantic OCS⁸, and the resulting empirical dataset comprises 3436 observations with a mean TOC value of 0.842%.

⁸ Boreholes include industry wells BR93, HC500, HC544, HC598, HC599, HC676, HC857, HC902, WI273, WI372, WI495, WI586, WI587, COST B-2, COST B-3, and DSDP/ODP scientific wells from Leg 1, Leg 11 (Boyce, 1972), Leg 43 (Cameron, 1979), Leg 44 (Myers, 1978), Legs 51 and 52 (White, 1979), Leg 76 (Sheridan et al., 1983), Leg 93 (Meyers, 1987), Leg 95 (Poag et al., 1987), Leg 150 (Mountain et al., 1994), Leg 164 (Paull et al., 1996), Leg 166 (Eberli et al., 1997), Leg 171 (Norris et al., 1998), and Leg 172 (Keigwin et al., 1998).

For every trial run, a TOC value is selected from the Weibull fit shown in Figure 17.

The Weibull probability density is:

$$f(x|a,b) = (a/b)(x/b)^{a-1} e^{-(x/b)^a}, x > 0$$

7.1.1.2 Sub-model: Methanogenic Production Function

The productivity, or rate at which methanogenic archaea convert organic carbon to methane in a given environment, is assumed to be a function of ambient temperature in that environment. An example of the particular function we use to represent the rate of methane produced by a collection of species in a given environment is shown in Figure 18, where:

(1) The intercept is productivity at the minimum value of the temperature domain (marked A). The value assumed by the intercept is a critical value because it *scales productivity at all temperatures*. In our model, the intercept captures the collective influence on the dependent variable (methane production rate) of all explanatory variables *other than temperature*.

(2) As temperature increases above its minimum, methane productivity increases monotonically over a finite temperature interval (marked B). This is the domain of Arrhenius' Law, an exponential growth law which declares that the rate of a chemical reaction doubles for every 10° C increase in temperature.

(3) Additional heat ultimately slows the rate of productivity. It peaks at a finite temperature (marked C). In the example shown in Figure 18, the shape of the rate function in a neighborhood of peak productivity is dictated by interactions among multiple species of methanogens, each contributing to the total mass of methane produced.

(4) As temperature continues to increase above peak productivity temperature, the rate of productivity rapidly declines (marked D).

(5) Finally, as with any biologic organism, there is a temperature limit beyond which organisms can no longer survive; biologic metabolism of organic carbon ceases—and so does biogenic methanogenesis (marked E).

Our model of methanogenesis begins with analysis of productivity of a single species under seafloor conditions. It is then extended to incorporate productivity by methanogenic communities in buried sediments. Modeling of productivity proceeds in three steps:

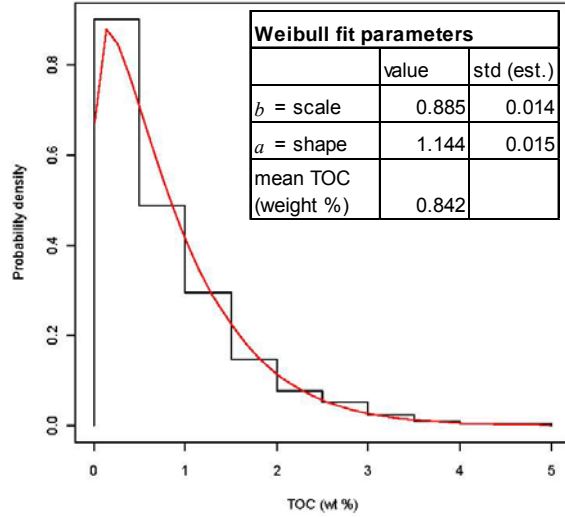


Figure 17. Histogram of Atlantic TOC data (weight %) and Weibull fit parameters.

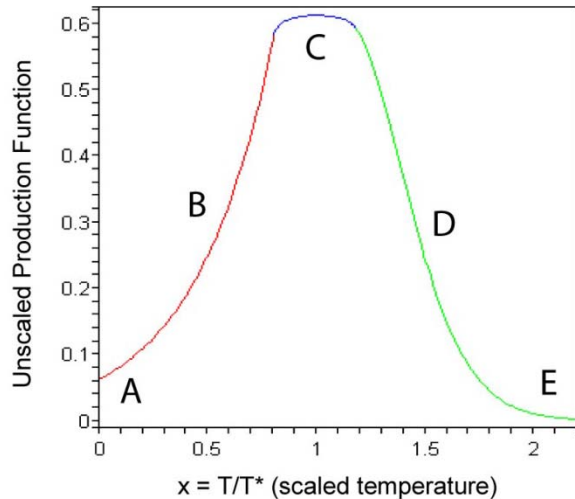


Figure 18. Methanogenic production (unscaled) shown as a function of scaled temperature. Letters A through E make reference to description in Section 7.1.1.2 of this report.

(1) Construct a rate function of temperature assuming that all methane is produced by a single species of archaea. This captures the basic dynamics of the process.

(2) Recognize that methanogenesis in marine sediments is most likely the collective contribution of a community of many species of methanogenic archaea. Modify the single-species function to reflect this.⁹

(3) Extend the model of productivity under seafloor conditions to include subsurface conditions. This is handled by modeling the intercept (“A” in Figure 18) to be a function of a ratio sediment permeability at the seafloor and sediment permeability at subsurface depths. As stated earlier, the intercept is a fundamental parameter—it directly scales the temperature/productivity function shown in Figure 18 above.

7.1.1.2.1 Maximum Initial Production

The maximum initial production (*MIP*) parameters are largely based on data presented by Price and Sowers (2004) that are used to interpolate productivity of methanogens at seafloor temperature. Results from the Price and Sowers (2004) data converted to grams per cubic meter per millions of years ($\text{g}/\text{m}^3/\text{my}$) show the distribution to have a mean of $2.63 \times 10^6 \text{ g}/\text{m}^3/\text{my}$ and standard deviation of 525×10^6 , a highly right skewed distribution. This initial distribution was modified to reflect an *MIP* with a mean of 35 and a standard deviation of 140 and modeled with a lognormal distribution (Figure 19) to reflect the skewness. The resultant model is:

$$MIP \sim \text{lognormal}(\log \text{ mean} = 3.555348, \log \text{ std dev} = 4.941642) \times 1,000,000$$

The *MIP* is drawn once for each trial. Thus, the same value is used for production from all lithologies in a given trial.

The next step in estimating production is to scale the *MIP* by the ratio of midpoint thickness permeability (*MidP_i*) in the *i*th ISO (lithology) to water bottom permeability (WBP), defined in the Section 7.1.1.2.2.1. Thus, the production intercept between the *i*th and *j*th lithology is

$$Int_{ij} = \min(MidP_{ij}/WBP, 1) \times MIP$$

7.1.1.2.2 Sub-model: Permeability

While temperature shapes the marginal rate of production of methane, the scale of the function is influenced by other variables – most prominently, water flux through the sedimentary environment. At seafloor conditions, water flux through the sediments in which methanogenic archaea live is at its maximum. Sediment compaction on burial diminishes permeability, ensuring that water flux declines as a function of sediment burial depth as well. The relationship between water flux and methanogenic productivity is direct; as water flux increases, so does productivity and vice versa. As we have no observations on water flux through sediments as a function of depth, we adopt permeability as an instrumental variable for it.

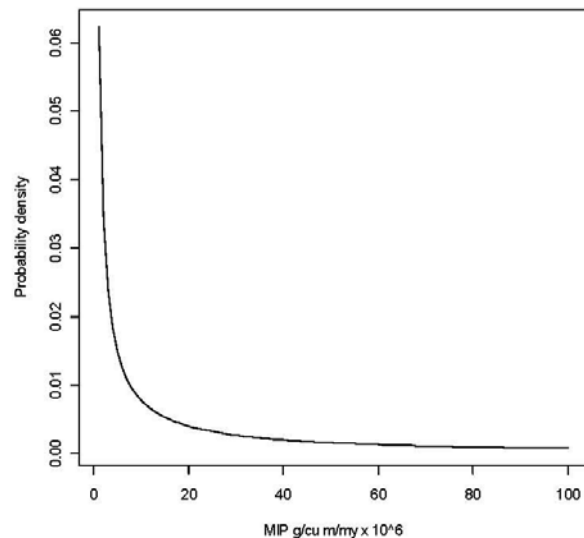


Figure 19. Model of maximum initial production of methane. Units are $10^6 \text{ g}/\text{m}^3/\text{my}$.

⁹ The single species rate function and the modified species function are described in detail in [OCS Report MMS 2008-004](#).

7.1.1.2.2.1 Permeability at Water Bottom (WBP)

To scale the change in permeability at depth, we first calculate the permeability of sediment at the seafloor:

$$\text{WBP} = (1000 * (1 - \text{SND})) + (593 * \text{SND})$$

where SND is fraction of sand in a given cell. This is a given input for each cell.

7.1.1.2.2.2 Sand Permeability as a Function of Depth

Data used to establish the relationship between sand permeability as a function of depth consisted of 9461 observations from the Gulf of Mexico. The fitting procedure consisted of the following three step approach:

1. Apply a Box-Cox transformation to the permeability data to make the distribution as symmetric as possible yielding $\hat{f}(Y | x)$, where Y is permeability in millidarcies and x is depth in meters. The Box-Cox parameter estimate $\hat{\lambda} = 0.1530$.
2. Then fit $\hat{f}(Y | x)$ to depth x using a regression model. This yields the model:

$$\hat{f}(Y | x) = 10.85 - 0.000258x$$

The residual standard error for this model is estimated to be 2.541.

3. Back transform $\hat{Y} = (\hat{\lambda} \hat{f}(Y | x) + 1)^{1/\hat{\lambda}}$ to obtain estimates of Y .

Residual standard error: 2.541 on 9367 degrees of freedom. Adjusted $R^2 = 10\%$. The fitted model at the mean is shown in Figure 20.

Then the sand permeability $MSSP_{ij} = (\hat{\lambda}(a + b \times MPT_{i,j}) + Error + 1)^{1/\hat{\lambda}}$.

See SandPermCoeff, Lambda, and SandPermError (column 1) in Setup.xls (Appendix A). $MPT_{i,j}$ is midpoint thickness from the top of lithology i to the bottom of lithology j .

7.1.1.2.2.3 Shale Permeability as a Function of Depth

First we model *shale porosity* as a function of depth. The relationship between porosity and depth is taken from Spinelli et al. (2004) as

$$P = \Omega M^\tau,$$

where P is porosity in decimal percent, M is midpoint depth in meters, $\Omega \sim N(0.84, 0.08^2)$, and $\tau \sim N(-0.125, 0.01^2)$.

John Grace (personal communication, December 19, 2006) recommended that the maximum value of porosity be 0.7. Thus, $P = \min(\Omega M^\tau, 0.7)$. The model is shown in Figure 21 at the mean values of parameters.

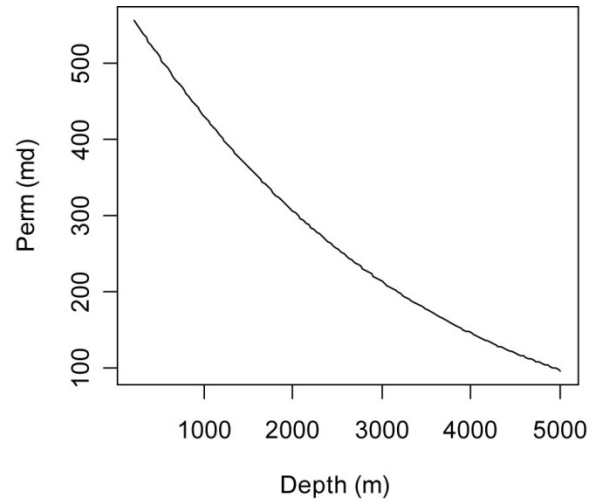


Figure 20. Sand permeability model at the mean versus depth.

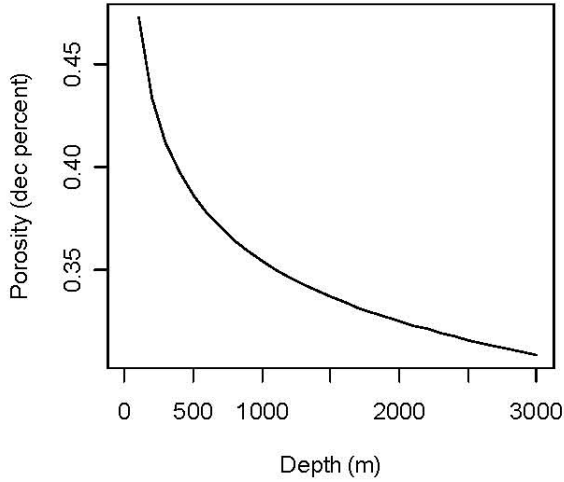


Figure 21. Shale porosity model at the mean versus depth.

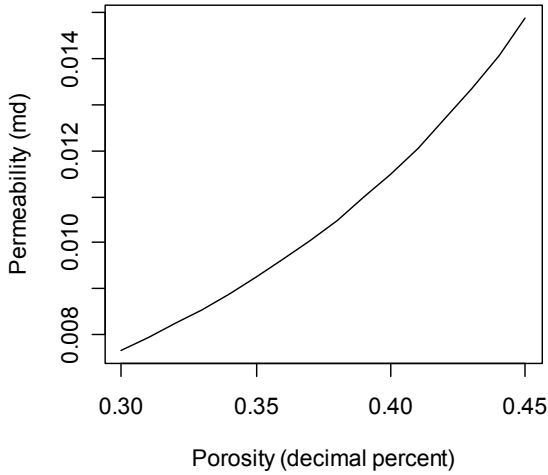
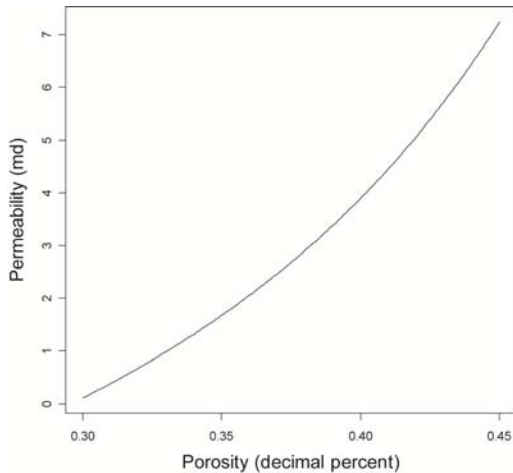


Figure 22. Permeability versus porosity model at the parameter means.



Next, we calculate shale permeability as a function of porosity (from Spinelli et al., 2004):

$$Pe = \nu e^{\omega(P/(1-P))}$$

where Pe is permeability in millidarcies (md), P is porosity in decimal percent (fraction), $\nu \sim N(0.0037, 0.00037^2)$, and $\omega \sim N(1.7, 0.17^2)$. Figure 22 shows the relationship between porosity and permeability at the parameter means.

Finally, the permeability as a function of depth is

$$Pe = \nu e^{\omega(\Omega M^r)/(1-\Omega M^r)}$$

As the range of shale permeability appears both too narrow and values too low, we rescale the shale permeability Pe as follows:

$$Pe \leftarrow \max(\{990 \times Pe - 0.00766\} - 0.2866, 0)$$

This re-scaling is supported by other work, such as Katsube and Connell (1998), who present a range of shale permeability from 0.003 to 15 md depending on pressure and other factors. Thus, 0.008 and 0.013 in the Spinelli relationship become 0.05 and 5.0 md, respectively. This model for Pe implies that $Pe = 0$ for porosity less than 0.31 (decimal percent), which corresponds to a depth of 3800 m. Note that a porosity of 0.45 corresponds to a depth of 147 m.

A graph showing the relationship between the rescaled permeability and porosity is given in Figure 23.

The shale permeability in the interval between lithologies i and j is:

$$MSHP_{ij} = O e^{\chi(MSHPR_{i,j}/(1-MSHPR_{i,j}))}$$

See Omicron (O) and Chi (χ) (column 1) in Setup.xls (Appendix A). $MSHPR_{ij}$ is the midpoint thickness shale porosity, lithologies (i, j).

Figure 23. Rescaled shale permeability versus porosity at the parameter means.

7.1.1.2.2.4 Average Rock Bulk (Midpoint) Permeability

The midpoint permeability is a function of fraction of sand in a cell (SND), midpoint sand permeability ($MSSP_{ij}$), and midpoint shale permeability ($MSHP_{ij}$).

$$MidP_{ij} = SND \times MSSP_{ij} + (1 - SND) \times MSHP_{ij}$$

7.1.1.2.3 Sub-model: Sediment Temperature

The temperature of buried sediment is found at any given depth in the model by applying a geothermal gradient (reported as an increase in °C per kilometer of depth below the seafloor) to a starting temperature that corresponds to the sediment temperature at the water bottom. The mathematics of this process are shown below. The development of the GTG input is described in Section 7.2.1.1 and in Appendix B.

7.1.1.2.3.1 Water Bottom Temperature

The water bottom temperature (WBT) provides the starting point from which sediment temperatures at depth are calculated. The data and fitted model are shown in Figure 24. The form of this sub model (also called seafloor temperature) is:

$$WBT = \begin{cases} 12.563 - 0.0071054 \times WD + \omega_1 & 150 \leq WD < 1000 \\ 1194 \times WD^{-0.780} \times e^{\omega_2} & 1000 \leq WD \leq 1444 \\ 4.1 + \omega_3 & WD > 1444 \end{cases}$$

where WD is water depth in meters and the error terms for the three models are:

$\omega_1 \sim N(\text{mean } 0, \text{ standard deviation } 0.62)$,

$\omega_2 \sim N(\text{mean } 0, \text{ standard deviation } 0.556)$, and

$\omega_3 \sim N(\text{mean } 0, \text{ standard deviation } 0.184)$.

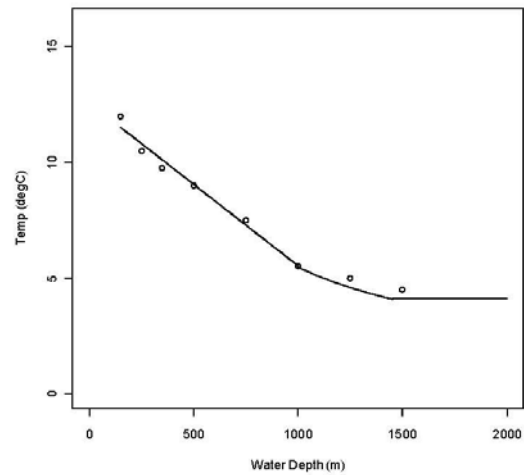


Figure 24. Water bottom temperature data and model.

7.1.1.2.3.2 Sediment Temperature

Consider two lithologies i and j , where j is the younger one. In order to compute a production function, it is necessary to know the top (SDT_{ij}) and bottom (SDB_{ij}) temperatures in the range between lithologies i and j . These estimates are computed using the following algorithm:

```

Let s = WBT(Cell,Trial)
DO 30 from j = 1 to 6
  SDTij = s
  DO 25 from i = j to 1, by -1
    SDBij = SDTij + GTG x MPTij
    if (i > 1) SDTi-1,j = SDBij
  END 25 loop
END 30 loop

```

where GTG is the geothermal gradient and MPT_{ij} is the midpoint lithology thickness in meters. There are six lithologies. So for example:

$$\begin{aligned}
SDT_{11} &= WBT \\
SDB_{11} &= SDT_{11} + GTG \times MPT_{11} \\
SDT_{22} &= WBT \\
SDB_{22} &= SDT_{22} + GTG \times MPT_{22} \\
SDT_{12} &= SDB_{22} \\
SDB_{12} &= SDT_{12} + GTG \times MPT_{12}
\end{aligned}$$

7.1.1.2.4 Sub-model: Asymptotic Conversion Efficiency

Calculation of the mass of methane produced, given a mass of organic carbon input, is done by looping through each of six stratigraphic units that cover the sedimentary column of each cell. Starting with the original deposition of organic carbon in any one of those units, the productivity function is integrated over a temperature interval corresponding to top and bottom depths of the unit to determine the amount converted to methane at a period in geologic time. At each time period, the cumulative amount of organic carbon converted to methane is calculated. The mass of organic carbon already converted is subtracted from the mass available for conversion in the next geologic time step. However, if the cumulative amount converted at any time step exceeds the estimated generation potential, production of methane ends, and no more is generated in the model for the remaining periods of geologic time.

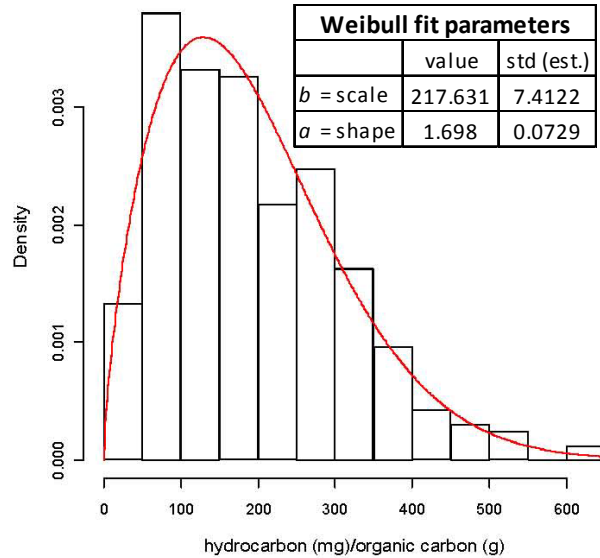


Figure 25. Atlantic quality (RockEval) data and Weibull fit parameters.

The susceptibility of organic carbon to transform into hydrocarbons is quantified by a procedure known as hydrous pyrolysis (also known by the commercial name of the apparatus used, RockEval), from which the limiting (asymptotic) value of organic carbon to hydrocarbon transformation is calculated. We use 332 observations from 21 Ocean Drilling Program (ODP) wells¹⁰ on the Atlantic margin to develop a Weibull fit by the method of moments to $OmtQual = (S1 + S2) * 100 / TOC$, where S1 and S2 values are unique to each observation¹¹. A histogram and Weibull fit to the quality data is shown in Figure 25, with a mean value of 194.2 mg/g. Note that the asymptotic conversion efficiency is multiplied by 0.001 in the generation model to express it as a fraction.

7.1.1.3 Allocation of Sediment Thickness to Deposition by Geologic Time Period

The thickness of the stratigraphic column in each cell in the study area is measured from the seafloor to the base of the Tertiary section (top Cretaceous). This thickness varies across the Atlantic OCS from 100 m to over 5000 m.

This thickness is directly measured or interpolated (via seismic data interpretation) and isolated in the assessment model input file as ISO 1 (seafloor to top Pliocene) and ISO 2 (top Pliocene to base of

¹⁰ ODP Leg 150 sites 902, 903, 904, and 905 (Mountain et al., 1994); ODP Leg 164 sites 991, 992, 993, 994, 995, and 997 (Paull et al., 1996); ODP Leg 171 sites 1049 and 1052 (Norris et al., 1998); ODP Leg 172 sites 1054, 1056, 1057, 1058, 1059, 1060, 1061, 1062, and 1063 (Keigwin et al., 1998).

¹¹ S1 = quantity of free hydrocarbons in the rock samples, in mg/g rock; S2 = quantity of hydrocarbons produced by kerogen cracking, in mg/g rock.

Tertiary)¹². The ISO 2 interval is then divided equally into five geologic units: Pliocene, Miocene, Oligocene, Eocene, and Paleocene. The geologic time intervals and durations of each unit are shown in Table 3. Each Monte Carlo trial divides the total sedimentary column in a cell into thicknesses of each of the six time/rock units. The mid-point depth of each unit at that trial is computed and recorded.

ISO	Epoch	Top (my)	Base (my)	Duration (my)
ISO1	Pleistocene	WB	1.95	1.95
ISO2'	Pliocene	1.95	5.05	3.10
ISO3'	Miocene	5.05	24.65	19.60
ISO4'	Oligocene	24.65	33.70	9.05
ISO5'	Eocene	33.70	55.00	21.30
ISO6'	Paleocene	55.00	65.00	10.00

Table 3. Chronostratigraphic units with corresponding age for the top and base of each unit (my = million years).

The primes in ISO 2' through ISO 6' reflect division of the original ISO 2. The thickness are $Thk_1 = \text{ISO } 1$, $Thk_i = \text{ISO } 2/5$, $i = 2, \dots, 6$. ISO 1 and ISO 2 are read in by cell in the input data file (not shown).

To estimate porosities and permeabilities of each unit at each time interval (at progressively deeper burial depths), it is necessary to compute the midpoint thickness MPT_{ij} between lithologies i to j . For example, $MPT_{1,3} = 0.5 \times Thk_1 + Thk_2 + 0.5 \times Thk_3$.

7.1.1.4 Generation Potential (GP)

The generation potential (GP) recognizes the fact that, at some point throughout the depositional and burial history of the i^{th} lithology, all of the TOC endowment (subject to the asymptotic conversion efficiency) may be converted to methane. The generation potential (calculated in grams) for the i^{th} lithology ($i = 1, \dots, 6$) is:

$$GP_i = TOC \times \text{OmtQual} \times Thk_i \times \text{CellArea} \times \text{SedDen} \times 1,000,000$$

where

- TOC is fraction of total organic carbon,
- OmtQual is the asymptotic conversion efficiency (a fraction) of TOC,
- Thk_i is the thickness of the i^{th} lithology in meters,
- CellArea is cell area in m^2 ,
- SedDen is sediment density at the seafloor in g/cc , and
- 1,000,000 is the number of cubic centimeters in a cubic meter.

TOC and OmtQual are model fits; their parameters can be changed in Setup (see Appendix A) as can CellArea and SedDen .

7.1.1.5 Incremental Generation (IG)

The incremental generation (calculated in grams) between the i^{th} and j^{th} lithologies for a given trial is:

$$IG_{ij} = \text{Int}_{ij} \times TOC \times \text{Age}_i \times \text{CellArea} \times \text{Ar}_{ij} / \text{GTG}$$

where

- Int_{ij} , CellArea and TOC are defined above,
- Age_i is the duration of i^{th} lithology in millions of years (my),

¹² The Atlantic input file also contains thickness measurements ISO3 (top Cretaceous to top Jurassic) and ISO4 (top Jurassic to top Basement); these units are not used in the Atlantic assessment model.

- Ar_{ij} is the integral over the mesa function (Figure 26) from bottom to top temperatures, and
- GTG is the geothermal gradient.

Arrhenius' Law is an exponential growth law which declares that the rate of a chemical reaction doubles for every 10°C increase in temperature. The Arrhenius' Law was modified to generate a smooth function (Figure 26), where the production rate peaks at 35°C and declines to a negligible value at temperatures above 70°C.

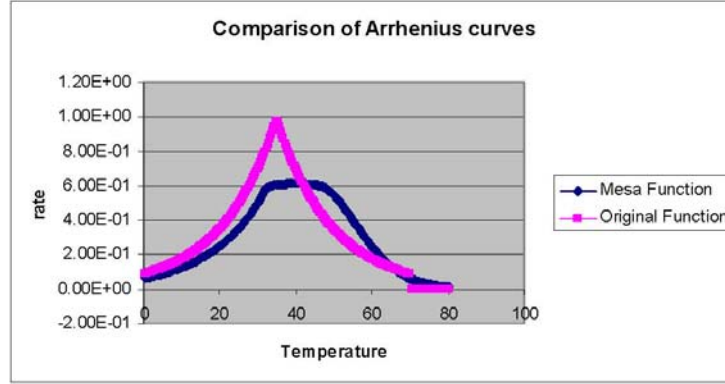


Figure 26. Comparison of Arrhenius law curves.

7.1.1.6 Resultant Generation

The final step in the methane gas generation model provides a comparison of the incremental gas generation (IG) from each chronostratigraphic unit to the generation potential (GP) of that same unit. The lower of the two values for each chronostratigraphic unit are retained and the results summed for the entire stratigraphic section of each model cell.

Let
$$IG_i = \sum_{j=i}^6 IG_{ij}, \quad i = 1, \dots, 6$$

then if $IG_i \leq GP_i$, $G_i = IG_i$, else $G_i = GP_i$ where G_i is the generation for the i^{th} lithology.

The resultant generation for a given cell-trial is:

$$G = \sum_{j=1}^6 G_i .$$

7.1.2 Migration Model

The gas migration model adopted for the Atlantic OCS is a simple one: gas is restricted to vertical migration. In general, the deepwater Atlantic OCS subsurface is dominated by gentle regional dip and relatively few features that would serve to focus gas migration, resulting in an environment that is likely dominated by vertical gas migration. However, we concur with observations made by Tucholke et al. (1977) and believe that in select areas of the Atlantic OCS, such as the positive relief anticlinal feature that comprises the Blake Outer Ridge, a not insignificant component of dip-driven (lateral) gas migration does take place. From a spatial modeling standpoint, the adaptation of an OCS-wide mechanism to recognize local lateral movements proved too difficult to model, thus the deployment of the ubiquitous vertical migration model.

The recognition that all gas generated in a model cell will not migrate to the HSZ invokes the need for some reduction of the volume of generated gas prior to emplacement as a charge to the HSZ. We employ

this reduction as a Trapping/Migration Efficiency (T/M) that is sampled from an uncertain distribution and applied to each model cell. The T/M accounts for gas not expelled from the source formation, gas trapped in route to the HSZ, and gas expelled at the seafloor, among others.

We model the T/M as three separate distributions (Figures 27 a-c), and invoke the presence (or absence) of a BSR at each model cell as a proxy to select from one of the three distributions. In model cells where we observe a “high confidence” BSR (Section 4.4), the model code will call a value from the richest T/M distribution (Figure 27c). In model cells where no BSR is observed (or where seismic data are not available), the model code will draw from the lowest T/M distribution (Figure 27a). The median T/M distribution (Figure 27b) is employed for model cells where a “moderate confidence” BSR has been identified.

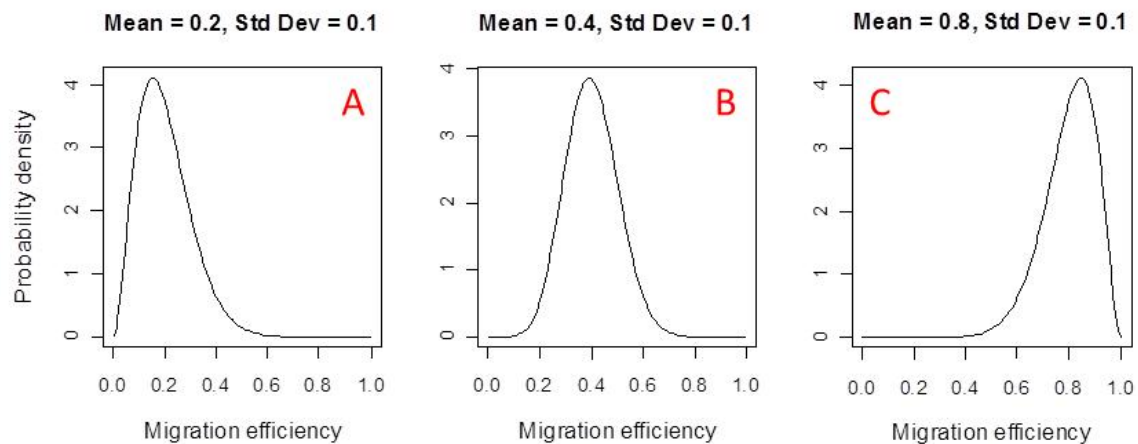


Figure 27. Trapping/Migration efficiencies modeled as beta distributions. (a) T/M applied to model cells with no BSR; (b) T/M applied to model cells with “moderate confidence” BSR; (c) T/M applied to model cells with “high confidence” BSR.

7.2 Container Module

The study area’s rock volume that is a candidate for formation of natural gas hydrate is estimated in two steps. First, we employ a model to estimate the “gross” HSZ. The gross HSZ covers that volume of rock in which pressure and temperature conditions permit the formation of gas hydrate, if available pore space and sufficient hydrocarbon charge are present. Second, we then remove a layer of the gross HSZ, starting at the seafloor and extending downward. In this layer, saturation of methane in ambient waters is believed to be below 100 percent. Where formation waters are undersaturated, hydrates will not form. Here we call a layer in which this condition is present the “undersaturated zone” (UZ). The gross HSZ, minus the UZ yields the net HSZ.

7.2.1 Gross Hydrate Stability Zone Thickness Model

Estimation of the gross HSZ is based on a basic relationship described by Milkov and Sassen (2001) (hereafter referred to as *M/S*). Their fundamental equation is an implicit function in which two relationships are set equal to each other to establish a phase boundary in temperature and pressure. For pressures less than that at the phase boundary and, simultaneously, temperatures greater than that at the phase boundary, methane will occur in gas phase. At pressures greater than the boundary and, simultaneously, temperatures below the boundary, methane molecules are trapped in frozen water molecules, forming gas hydrate. Pressure at a point on or below the seafloor is taken to be a function of its depth below mean sea level (i.e., water depth plus depth below seafloor). Temperature at that point is the sum of temperature at the seafloor plus depth below seafloor times the GTG.

The M/S equation is solved for the depth below the seafloor at which ambient temperature and pressure are equal to the value of the phase stability expression. This depth marks the bottom (in meters below seafloor) of the gross hydrate stability zone and thereby defines its gross thickness. In any model cell, if the pressure is too low and/or temperature too high, the thickness of the gross HSZ will equal zero.

The BOEM model uses a modified version of M/S equation that consists of three sub-models: geothermal gradient, seafloor temperature (discussed in Section 7.1.1.2.3.1) and phase stability.

HSZ is a zero of:

$$f(HSZ | WD) = -[GTG \times \frac{HSZ}{1000}] - WBT + [\delta \times \ln(HSZ + WD) - \gamma]$$

where,

- WD = water depth (meters)
- GTG = geothermal gradient ($^{\circ}C/km$)
- HSZ = thickness of the hydrate stability zone (meters)
- WBT = water bottom temperature ($^{\circ}C$)
- δ = slope of phase stability equation
- γ = intercept of phase stability

The parameters γ and δ are discussed in the phase stability Section of this report (Section 7.2.1.2).

The solution is by Newton-Raphson, where the first derivative of f with respect to HSZ thickness is:

$$f' = \partial f / \partial (HSZ) = -(GTG / 1000) + \delta / (HSZ + WD).$$

Before beginning Newton-Raphson iterations, a check is made to see if any positive roots exist. Let

$$a = WBT + \gamma - \delta \times b \times WD$$

$$b = GTG / (1000 \times \delta)$$

where WBT is the estimated water bottom temperature. Let $x_m = 1/b - WD$ be the value of HSZ where $f(HSZ|WD)$ is maximum, again conditioned on WD . Let

$$g_m(x_m | WD) = f(x_m | WD) / \delta$$

be the maximum value of f . Then

$$g_m = \log(x_m + WD) - (a + bx_m).$$

Let $g_0 = \log(WD + 0.00000001) - a$ the value of f at $HSZ = 0$. If $((g_m < 0) \vee ((x_m \leq 0) \& (g_0 < 0)))$, f has no positive roots and $HSZ = 0$, otherwise, Newton-Raphson iteration is begun.

A simplified version of the procedure is as follows. An initial estimate of HSZ is made, call it x_0 . The first approximation to the solution is

$$x_1 = x_0 - f / f'$$

A check is made to see if x_1 is within epsilon of a solution or the number of specified interactions is exceeded. If not, the procedure is repeated, i.e.

$$x_2 = x_1 - f / f'$$

The resultant netHSZ = min(HSZ as computed above, thickness of i^{th} lithology).

7.2.1.1 Geothermal Gradient (GTG)

The underlying data points ($n = 47,379$) used to construct the GTG histogram (Figure 28) were derived by solving the M/S equation for GTG (rather than HSZ) in areas of seismic BSR on the Atlantic OCS, using the assumption that the thickness of the HSZ is known (or inferred) from the direct indicators in the seismic data. Modeled GTG values were compared to physical temperature measurements to verify the relative accuracy of the calculations. The detailed process of developing this data set is described in Appendix B. A beta fit to the scaled (0 to 1) data is shown in Figure 29.

A GTG random deviate is distributed as $15 + 30 \text{Beta}(8.0583, 5.2975)$ with range (15, 45). The mean of this fitted distribution is 33.101 and the standard deviation of 3.853.

7.2.1.2 Phase Stability Submodel

In addition to pressure and temperature, the thickness of the HSZ is dependent upon the molecular composition of the gas that combines with water to form gas hydrate. In the M/S equation that we employ to calculate HSZ thickness, the variable composition of the gas is captured in the delta (δ) and gamma (γ) components.

The basic phase stability equation model ($PsE = \delta \ln(HSZ + WD) - \gamma$) is derived from Milkov and Sassen (2001) equations 3, 4 and 5. Table 4 contains values for delta (δ) and gamma (γ) at three values of methane content, as reported in Milkov and Sassen (2001). These values (Table 4) are derived from negative exponential fits to temperature – depth relationships derived by Sloan (1998).

The gamma and delta corresponding to a $\text{CH}_4 = 99\%$ are 45.234 and 8.243 respectively. They were found by spline interpolation to the values in Table 4.

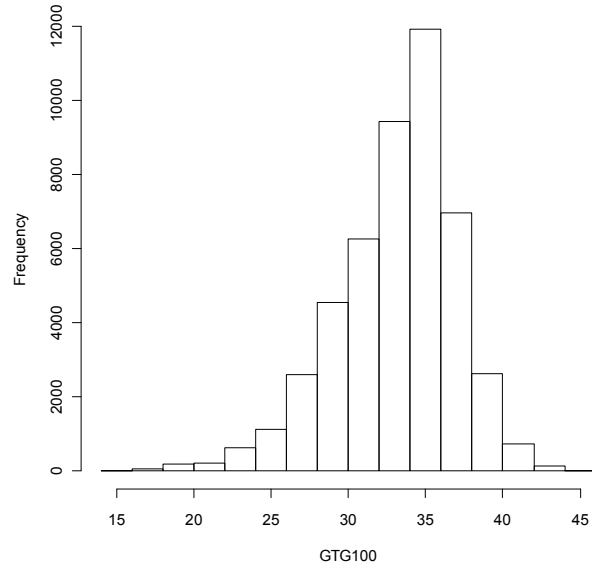


Figure 28. Histogram of estimated GTG observations. Horizontal axis units are $^{\circ}\text{C}/\text{km}$.

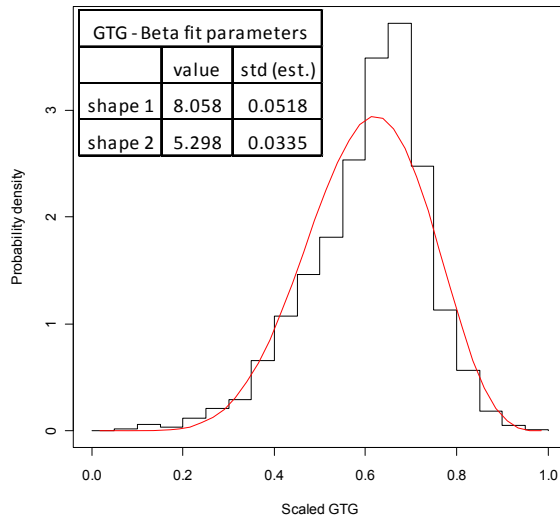


Figure 29. Histogram of scaled GTG data and beta fit parameters.

CH4 (%)	Delta δ	Gamma γ
100	8.9	50.1
95.9	7.1	33.9
90.4	6.7	27.6

Table 4. Delta and Gamma values.

The estimated parameters for CH₄ = 99% are shown in the Table 5, and the beta fit parameters to delta and gamma are shown in Table 6.

Parameter	Beta means	Parameters			
		p1	p2	p3	p4
γ	0.9900	1.0000	0.0101	40.2840	5
δ	0.0100	0.0101	1.0000	8.2330	1

Table 5. Delta and gamma parameters corresponding to CH₄ = 99% where p1 and p2 are the estimated shape parameters. Estimated parameters for beta fits to delta and gamma are given in Table 6.

Parameter	Equation	Mean	Min	Max
γ	γ (est) = p4 x beta(p1,p2)+p3	45.2340	40.2840	45.2840
δ	δ (est) = p4 x beta(p2,p1)+p3	8.2430	8.2330	9.2330

Table 6. Estimated parameters for delta and gamma beta distributions.

The domain of the distribution associated with the gamma parameter was increased by a multiple of 5 to provide a more realistic estimate of the variance. It is denoted by p4 in Table 5. The means shown in Table 6 were held constant by adjusting an additive constant p3 (Table 5). Note that the variance of the delta parameter was not changed because doing so resulted in unreasonably large values of HSZ thickness.

The resultant distributions of gamma and delta are shown in Figures 30 and 31, respectively.

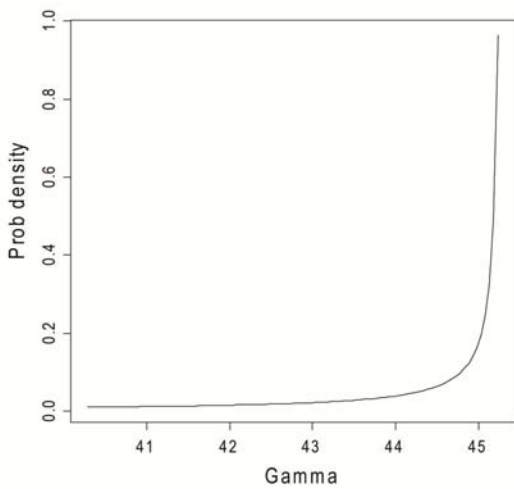


Figure 30. Distribution of gamma parameter estimate.

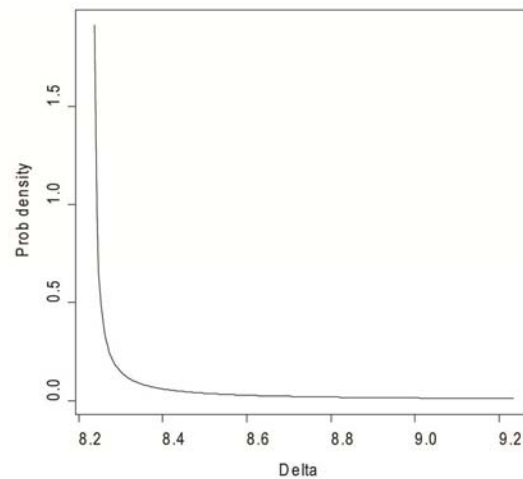


Figure 31. Distribution of delta parameter estimate.

7.2.2 Undersaturated Zone Thickness Model

Several processes may work to inhibit gas hydrate formation in the section immediately below the seafloor and extending some uncertain distance downward. Limited upward migration of methane, downward intrusion of undersaturated ocean waters, and sulfate reduction through excessive biologic activity all serve to drive methane concentration below saturation and prevent the formation of gas hydrate. This section we refer to as the undersaturated zone (UZ).

In the Atlantic OCS, we make no attempt to model the UZ thickness as a local or spatial phenomenon. Rather, for every trial we draw a value from the scaled beta distribution shown in Figure 32. This symmetric distribution has a mean of 200 m and a standard deviation of 141.4 m.

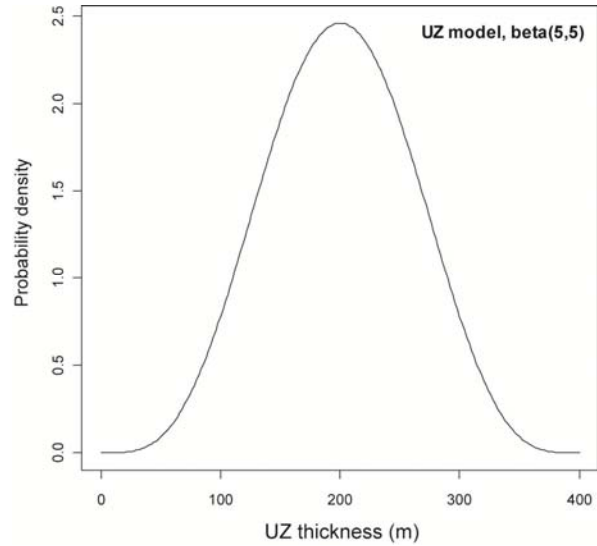


Figure 32. Beta model of the UZ thickness (mean = 200 m, std. dev. = 141.4 m).

7.2.3 Net Hydrate Stability Zone Thickness Model

The final calculation in the Container module yields the net HSZ, or that thickness of stratigraphic section capable of hosting gas hydrate. Here we remove the UZ thickness from the gross HSZ thickness and retain a net HSZ thickness. The model code reads:

$$\text{NHSZ} = \max(\text{HSZ} - \text{UZT}, 0)$$

where NHSZ is the net HSZ, HSZ is the gross HSZ and UZT is the undersaturated zone thickness.

7.3 Concentration Module

The Concentration module will yield, for every model cell, a calculation of that percent of the bulk rock volume in the net HSZ that will contain gas hydrate, conditional on the delivery of a sufficient gas charge. We model the available pore space by recognizing two end member lithologies (sand and shale) and assign some gas hydrate saturation to each lithologic unit by a selection from an uncertain distribution.

7.3.1 Porosity from shallow sand (SSP)

Porosity from shallow sand is estimated from GOM well KC151 data (Figure 33). The model of shallow sand porosity as a function of net HSZ midpoint depth (d) in meters is shown below.

$$\text{Fitted model plus error: } \text{SSP} = \text{SSH1} \times \exp(\text{SSH2} \times d(\text{m})) + \varepsilon$$

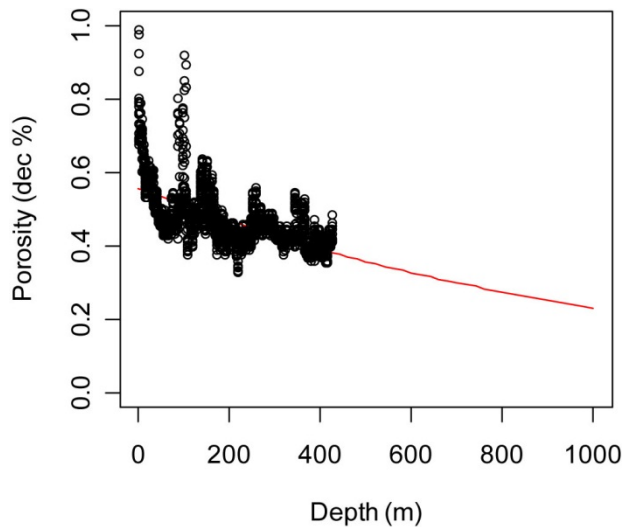


Figure 33. Porosity of shallow sand versus depth (meters below seafloor).

If SSP < 0, SandPor = 0
 If SSP > 1, SandPor = 1

Coefficient values for SSH1 and SSH2 are shown in Table 7 below.

	Estimate	Std. Error	t value	Pr(> t)
SSH1	0.5583	2.42E-03	230.98	<2e-16
SSH2	-8.93E-04	1.95E-05	-45.91	<2e-16

Table 7. Error coefficients for shallow sand porosity calculation.

The residual standard error is 0.05839 on 2,798 degrees of freedom. The error distribution is assumed to be normal. The correlation between parameter estimates is -0.838.

7.3.2 Porosity from shallow shale (SHP)

A shale porosity model developed by Hamilton (1976) has been modified here to ensure that shallow shale porosity falls between 0 and 1. Full details of these modifications are provided in Appendix C of this report. The resultant form of the model without error is:

$$SHP_o(d) = \frac{1}{1 + \exp\{\hat{\alpha} + \hat{\beta} \times d\}}$$

where d is the midpoint depth in meters. By matching the Hamilton (1976) model to the logistic equation we estimated, $\hat{\alpha} = -0.71956$ and $\hat{\beta} = 0.001756$. The error $\varepsilon \sim N(0, 0.015^2)$ is from Hamilton. These quantities are read from the Setup input sheet. The resultant model is

$$SHP(d) = \frac{1}{1 + \exp\{-0.71956 + 0.001756 \times d + \varepsilon / (SHP_o(d) \times (1 - SHP_o(d)))\}}$$

The graph of $SHP_o(d)$ for depths d from 0 to 2500 meters is shown in Figure 34, and a sample of model standard deviations as a function of depth is shown in Table 8.

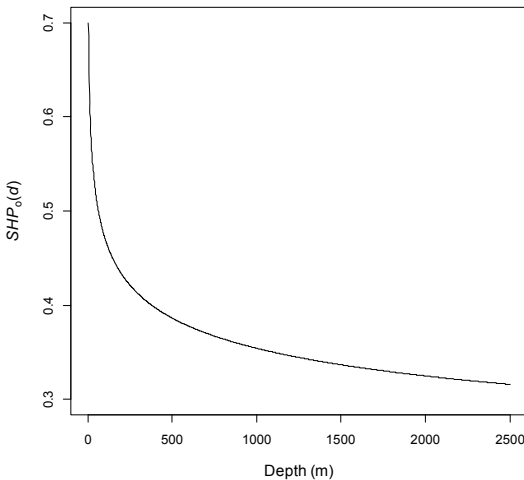


Figure 34. Logit function for porosity (y axis) as a function of depth (x axis) in meters.

Depth (m)	Porosity Logit Model	Std Dev ε	Porosity Hamilton Model
0	0.673	0.068	0.7196
100	0.633	0.065	0.642
500	0.460	0.060	0.405
750	0.355	0.066	0.315
1000	0.262	0.078	0.270
1250	0.186	0.099	0.270
1500	0.128	0.134	0.315
1750	0.087	0.189	0.405
2000	0.058	0.276	0.540
2250	0.038	0.410	0.720
2500	0.025	0.619	0.945

Table 8. Porosity estimate as a function of depth compared with Hamilton model.

The standard deviations in the above table are not a monotonic function of depth because the product of porosity times one minus porosity is not monotonic, as porosity traverses 0 to 1.

7.3.3 Methane Saturation of Volume of Total Void Space

The steps above result in, for each trial and cell, a percent of bulk rock volume of the net HSZ that is occupied by void space. The percent of void space that is occupied by methane hydrates is a function of lithology; this is hydrate saturation.

Undoubtedly, a number of factors will influence the magnitude of gas hydrate saturation in a porous reservoir, including capillary entry pressure, permeability, lithologic heterogeneity, availability of sufficient charge, migration pathways, top seal, etc. Our model does not include recognition of the various petrologic and hydrologic uncertainties that will influence the gas hydrate saturation. Rather, we have assembled empirical gas hydrate saturation data derived from well data and sample from that uncertain quantity for each model trial run.

Hydrate saturation is estimated separately for sand and shale.

7.3.3.1 Hydrate saturation in sand (SatS)

Gas hydrate saturation data from sand dominated reservoirs has been assembled from GOM Joint Industry Project (JIP) wells, GOM Alaminos Canyon (AC) 818 #001, Mallik M5L38 (Mackenzie Delta, NWT Canada), and the Northwest Eileen State-2 (ANWE2) and Mount Elbert well on the North Slope of Alaska. A histogram of the interpreted saturation values, the fitted beta curve, and the parameter estimates based upon maximum likelihood estimation of beta fit are shown in Figure 35. Shape parameters are read from the Setup file (Appendix A). The mean value of SatS is 0.65 and standard deviation 0.153. Thus, $SatS \sim \text{Beta}(5.6535, 3.0424)$.

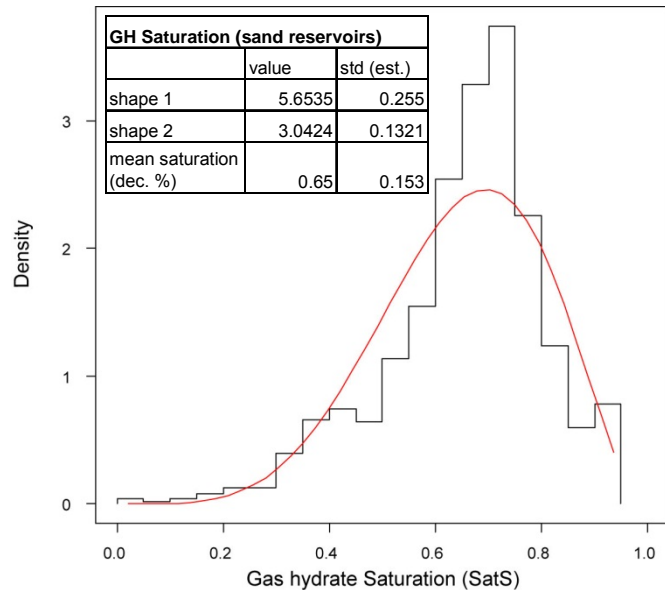


Figure 35. Histogram from combined gas hydrate saturation in sand and beta fit (red line).

7.3.3.2 Hydrate saturation in shale (GHS)

The following analysis of gas hydrate saturation in mud-dominated reservoirs is based upon saturation interpretations from wells in the deepwater GOM (JIP Leg I and Leg II), the Blake Ridge in the Atlantic OCS, and Hydrate Ridge in the Pacific OCS. The negative exponential with mean of 0.04 is a graphical fit to the histogram of the combined distribution (Figure 36).

The probability density is

$$f(GHS) = (1 / 0.04)e^{-GHS/0.04}, GHS \leq 1.$$

Thus, random variates from $GHS \sim -\hat{\mu} \log_e(\text{uniform}(0,1))$.

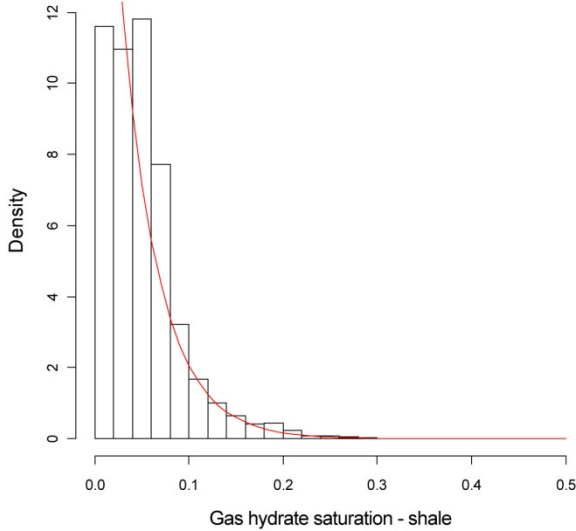


Figure 36. Histogram of GHS and fitted exponential distribution.

7.3.4 Total Saturated Void Space

The *saturation in sand concentration* (SSC_i) for the i th trial is

$$SSC_i = SSP_i \times SatS$$

where SSP_i , as previously defined, is the shallow sand porosity and SatS is the hydrate saturation in sand. SSP_i is computed anew for each trial. At the mean values for SSP (at a depth of 300 m) and SatS, $SSC = 0.730 \times 0.65 = 0.475$.

The *saturation in shale concentration* (SHC_i) for the i th trial is

$$SHC_i = SHP_i \times GHS$$

where SHP_i is the shale porosity for the i th trial and GHS is the hydrate saturation in shale. At the means of SHP (for a depth of 300 m) and GHS, $SHC = 0.672$ (mean porosity) \times 0.0334 (mean saturation) = 0.0224.

Finally the *total saturated void space* (TVS) for the i th trial, as a decimal between 0 and 1, available for charging is:

$$TVS_i = Sand * SSC_i + (1 - Sand) * SHC_i$$

where sand is expressed as a percent of sand plus shale, on input, and converted to a fraction in the Concentration module. Note that TVS is sometimes referred to as “saturation”.

7.4 Integration Module

The final step in the modeling routine requires a comparison of the volume of charge delivered to the HSZ and the volume of the accommodation space available in the HSZ. The smaller of the two values is retained as the volume of in-place methane hydrate in a model cell at reservoir temperature and pressure conditions.

This volume is then converted to standard temperature and pressure (STP) and reported in this convention. Finally, volumes of in-place gas hydrate in individual cells are aggregated to provide frequency distributions for the larger geographic area of the Atlantic OCS.

7.4.1 Volume Computation

The square cell used in the Atlantic model is 3,000 m on a side. The volume computation is described in the following steps where X refers to charge and Y the container:

Let X_1 = charge (g) at reservoir temperature and pressure (RTP), and

let $X_2 = (X_1 \times 0.001396) \text{ m}^3$ at STP

where the following expression converts grams to cubic meters:

$$0.001396 = 22.4 \text{ liters/mole} \times (1/(16.0425 \text{ g/mole})) / (1000 \text{ liters/m}^3)$$

Let $X_3 = X_2/fvf$ (m^3) at RTP, where fvf is the formation volume factor,

Let $Y =$ container size (m^3) at RTP
 $= \text{NetHSZ (m)} \times 3000^2$ (m^2) \times Saturation

Then if,

$X_3 > Y$ then $\text{vol} = Y$

else $\text{vol} = X_3$

Finally to obtain volume at standard temperature and pressure (STP), $\text{vol} \leftarrow \text{vol} \times fvf$

7.4.2 Formation volume factor (fvf) – volume at the surface

Once the volume of gas hydrate in place at reservoir temperatures and pressures is determined, it must be converted to volume at STP. This conversion accommodates the effect of the changes of gas temperature and pressure on gas volume, the deviation of the gas from ideal, and the range of clathrate cage occupancy. The conversion factor (equivalent to the formation volume factor in conventional petroleum engineering calculations) comes into the model as an uncertain quantity.

The distribution for fvf (Figure 37) has a mean of 164 and standard deviation of 5.13 and is represented by the following expression:

$$fvf \sim 139 + 33 * \text{Beta}(5, 1.6)$$

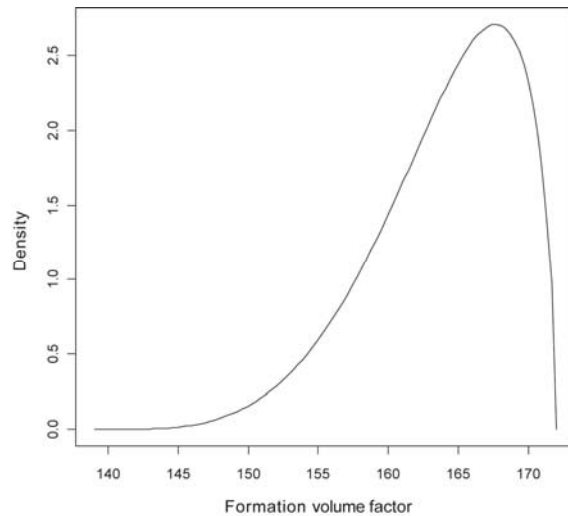


Figure 37. Distribution of fvf fit to a beta distribution and scaled to fvf range (139, 172).

8.0 RESULTS

At the end of each assessment model trial run, the in-place volume of gas hydrate (at STP) is recorded for each of the 57,066 model cells¹³. The in-place volume for each model cell is then aggregated to the larger geographic area of the Atlantic OCS, providing a single assessment of the in-place volume of gas hydrate for the Atlantic OCS study area. The above steps are repeated for 1,000 model trials and the in-place volume (at the cell level and OCS level) is recorded for each. The results can then be displayed as a distribution that reflects the uncertainty associated with the introduction of many of our model components.

A summary of in-place results after 1,000 trials is shown in Table 9. The mean in-place volume for the Atlantic OCS is 614 trillion cubic meters (equivalent to 21,702 trillion cubic feet). The complete distribution of in-place resources on the Atlantic OCS (0% to 100% cumulative probability) is shown in Figure 38. The mean in-place volume is presented in map view in Figure 39 (also shown as Figure 16).

¹³ Also recorded for presentation are the outputs from the three process modules (Charge, Container, and Concentration).

Statistic	Hydrate Concentration (decimal)	Total Net HSZ (trillions of m ³)	Total Hydrate Charge (trillions of m ³)	Total In-Place Volume (trillions of m ³)	Total In-Place Volume (trillions of ft ³)
Min.	0.015	4482	1.90	1.76	62.13
5%	0.034	10208	63.44	58.22	2056.10
25%	0.048	15598	363.49	280.08	9890.78
50%	0.060	19175	836.33	530.16	18722.41
Mean	0.064	19624	1463.83	614.54	21702.00
75%	0.075	23647	1956.19	845.19	29847.53
95%	0.103	29781	5117.93	1483.82	52400.36
Max.	0.168	40655	13173.50	3261.36	115173.30
Var.	0.000	34606400	3048820.00	199824.00	7056684.65

Table 9. Distribution of results from the four primary Modules of the BOEM gas hydrate assessment model.

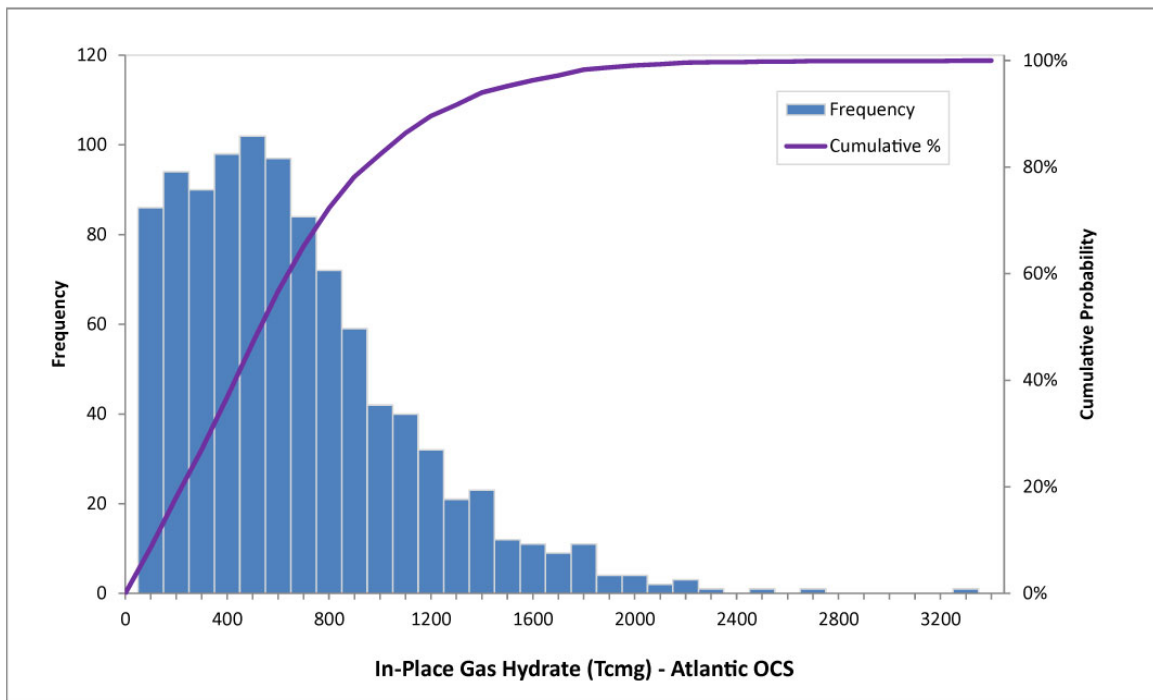


Figure 38. Distribution of in-place gas hydrate resources, Atlantic OCS. Units are trillion cubic meters.

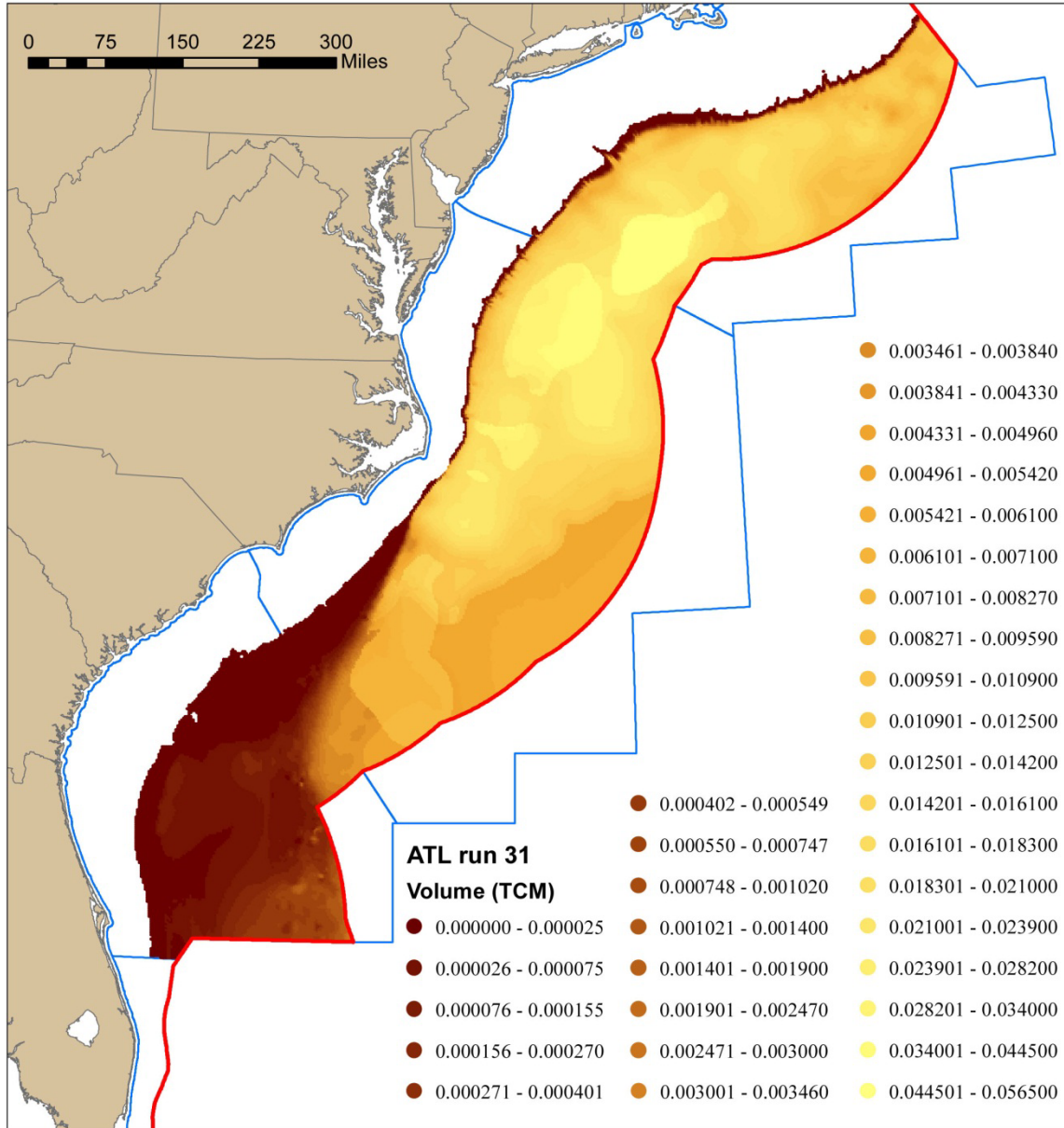


Figure 39. Map view of the mean in-place gas hydrate volume. Units are trillion cubic meters (1×10^{12} m³) of methane per 9 km² model cell expressed at surface temperature and pressure.

8.1 Sand Reservoirs

At the time of this publication, the in-place resources assessed on the Atlantic OCS have not been subjected to further modeling that could predict the technically- and economically-recoverable components of the resource base. However, based on preliminary field tests in the Arctic and reservoir simulation studies conducted for BOEM, we believe that that gas hydrate is technically recoverable from most sandstone reservoirs. With this in mind, we present a subset of the in-place resources by lithology of the sediment host, with the assumption that this is a necessary first step on the road to a full technically-recoverable analysis.

In the Arctic regions of North America, several advanced field projects have characterized production potential from gas hydrate in sand reservoirs in a permafrost environment. A joint effort in 2008 led by Canadian and Japanese researchers at the Mallik well site located in the Mackenzie Delta, Northwest Territories of Canada, obtained sustained gas flow to the surface from a gas hydrate reservoir (Kurihara et al., 2010). Under carefully controlled conditions over a six day period, a stepwise reduction in bottomhole pressure stimulated gas flow rates that averaged 70,000 - 100,000 ft³ per day. At the Mount Elbert well site in the Milne Point area of the Alaskan North Slope, a joint effort led by BP Alaska Exploration, DOE, and the USGS completed a gas hydrate test well in 2007. In addition to confirming the validity of pre-drill seismically-based predictions of gas hydrate occurrence, fluid and reservoir flow-properties data were obtained through the deployment of a wireline formation testing tool in the well (Anderson et al., 2011).

The most recent Arctic project (February – April, 2012) saw the completion of the Ignik Sikumi #1 gas hydrate field trial well from an ice pad in the Prudhoe Bay Operating Unit on the North Slope of Alaska. In this production test, a mix of nitrogen and carbon dioxide was injected into the wellbore and gas flow from a gas hydrate sandstone reservoir was established. Overall, the well produced for 30 days during the 38-day flow-back period, with peak rates as high as 175,000 ft³ per day and cumulative gas production approaching one million standard cubic feet. The CO₂ exchange project is a joint effort between DOE and ConocoPhillips, with additional support from the Japan Oil, Gas and Metals National Corporation (JOGMEC).

The BOEM in-place assessment model structure provides an opportunity to report resources by sedimentary host. Based on the recent test results that suggest sandy reservoirs offer the best chance for near-term production, the in-place results of this assessment are presented here as a mean in-place volume in sandstone reservoirs. Mechanically, this is accomplished by determining the fractional measure of void space available for saturation in sands per cell, then applying this fraction to the mean volume captured in the in-place model run. This fractional methodology is applied to each cell in the Atlantic study area.

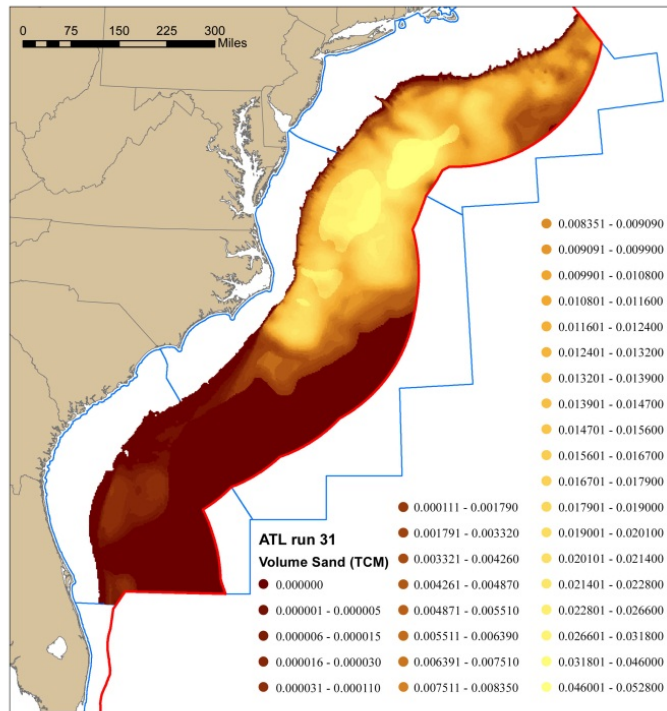
Void space available for saturation in sands and shales is determined from the product of porosity, hydrate saturation, and sand percent. Porosities for sands and shales are calculated (as a function of depth) at the mid-point depth of the net HSZ. Hydrate saturation of the available pore space is taken as the mean value of the saturation distributions described earlier in the methodology report (0.65 for sands and 0.04 for shales). The sand percent is a single value for each cell determined from the sand distribution maps described in the Spatial Inputs Section of this report (Section 4.3).

The workflow described above provides for each model cell, by lithologic facies, a unitless measure of the void space available for gas hydrate saturation. The total void space available for gas hydrate saturation per cell is the sum of the sand and shale values. The percent of this void space in sand reservoirs per cell is then calculated as the sand void divided by the total void. The product of the sand void fraction and the mean hydrate volume by cell equals the amount of hydrate in sand reservoirs by cell.

Using this workflow, the mean estimate of gas hydrate in-place in sand reservoirs in the Atlantic OCS is 447 TCM (~ 15,785 TCF). Only the mean value is reported, as the void space available for gas hydrate saturation in sand is calculated in a non-stochastic manner. Additionally, this fractional value is only applied to the mean estimate of the total in-place resource volume. Map view of these results is shown in Figure 40. The mean sand-only volume exceeds 70 percent of the mean in-place value generated for all reservoirs¹⁴.

¹⁴ The ratio of gas hydrate in-place in sand reservoirs versus that in-place in shale reservoirs for the Atlantic OCS is significantly higher than that reported for the 2008 GOM assessment, where ~30% of total resources reside in sands. The primary modeling factor driving this change is the reduction of predicted gas hydrate saturation in shale reservoirs from a mean of 10% (2008 GOM) to a mean of 4% (Atlantic - this study).

Figure 40. Map view of the mean in-place gas hydrate volume in sand reservoirs only. Units are trillion cubic meters ($1 \times 10^{12} \text{ m}^3$) of methane per 9 km^2 model cell expressed at surface temperature and pressure. Note that this value is calculated using a deterministic approach.



8.2 Model Calibration

Detailed in-place gas hydrate volume estimates by Collett and Ladd (2000) are available on the Atlantic margin on the Blake Outer Ridge, in the immediate vicinity of subsurface well control acquired as part of ODP Leg 164 (Paull et al, 1996). We offer a comparison of the results from this assessment to those published results in Appendix D.

8.3 Previous Resource Estimates

The United States Geological Survey (USGS) published a comprehensive assessment of in-place gas hydrate resources for the entire United States in 1995 (Collett, 1995). For the 1995 study, the Atlantic OCS was divided into a Northeastern play area and a Southeastern play area. The following table (Table 10) documents the results of the USGS assessment on the Atlantic OCS.

USGS 1995 Assessment Results	Estimated in-place natural gas resources (trillions of ft ³)					
	Mean	F95	F75	F50	F25	F5
Northeastern Atlantic Ocean play	30,251	0	0	14,128	49,448	109,491
Southeastern Atlantic Ocean play	21,580	6,464	11,656	17,660	27,196	49,448

Table 10. In-place gas hydrate resources on the Atlantic OCS (modified after Collett, 1995).

The combined mean resources of the Northeastern and Southeastern play areas from the 1995 assessment effort (51,831 tcf; 1,466 tcm) are greater than the results of the current BOEM study (614 tcm mean in-place). The major difference between the two assessments - other than the modeling approach - is the interpreted saturation of gas hydrate in fine-grained sediment. At the time of the 1995 publication, few marine gas hydrate data points existed in the world. Now, we have the benefit of the results from several targeted gas hydrate drilling programs, including those obtained during ODP Leg 164 on the Blake Outer Ridge.

8.4 Disclaimer

The BOEM in-place gas hydrate model incorporates varying levels of uncertainty at all levels of input. At this time, the results are not intended to describe commercial or potentially-commercial gas hydrate prospects or accumulations in any specific location, nor should they be used as an indicator of economic feasibility of any given model cell, OCS tract, or geographic area.

9.0 REFERENCES

Amato, R. V. (ed), 1987, Shell Baltimore Rise 93-1, Geological and Operational Summary, US Department of the Interior, Minerals Management Service, Atlantic OCS Region, OCS Report MMS 86-0128.

Anderson, B. J., Hancock, S., Wilson, S., Collett, T., Boswell, R., and Hunter, R. 2011, Formation pressure testing at the Mount Elbert Gas Hydrate Stratigraphic Test Well, Alaska North Slope: Operational summary, history matching, and interpretations, *Marine and Petroleum Geology* v. 28, Issue 2, p. 478-492.

Boyce, R.E., 1972, Carbon and carbonate analyses, Leg 11, *in* Hollister, C. D., Ewing, J. I. et al., 1972, Initial Reports of the Deep Sea Drilling Project, Volume XI. Washington (U.S. Government Printing Office), p. 1059-1071.

Cameron, D.H., 1979, Grain-size and carbon/carbonate analyses, Leg 43, *In* Tucholke, B. E., Vogt, P. R., et al, 1979. Initial Reports of the Deep Sea Drilling Project, v. 43: Washington (U.S. Government Printing Office), p. 1043-1047.

Collett, T.S., 1995, Gas hydrate resources of the United States, *in* Gautier, D.L., Dolton, G.L., Takahashi, K.I., and Varnes, K.L., eds., 1995 National assessment of United States oil and gas resources on CD-ROM: U.S. Geological Survey Digital Data Series 30.

Collett, T.S., and Ladd, J., 2000. Detection of gas hydrate with downhole logs and assessment of gas hydrate concentrations (saturations) and gas volumes on the Blake Ridge with electrical resistivity log data. *In* Paull, C.K., Matsumoto, R., Wallace, P.J., and Dillon, W.P. (Eds.), *Proc. ODP, Sci. Results*, 164: College Station, TX (Ocean Drilling Program), 179–191. [doi:10.2973/odp.proc.sr.164.219.2000](https://doi.org/10.2973/odp.proc.sr.164.219.2000)

Dunkel and Piper, 1997, 1995 National Assessment of United States Oil and Gas Resources; Assessment of the Pacific Outer Continental Shelf Region, OCS Report MMS 97-0019.

Eberli, G.P., Swart, P.K., Malone, M.J., et al., 1997, Proc. ODP, Init. Repts., 166: College Station, TX (Ocean Drilling Program).

Hamilton, E.L., 1976, Variations of density and porosity with depth in deep-sea sediments: *Journal of Sedimentary Petrology*, v. 46, no. 2, p. 280-300.

Katsube, T.J. and Connell, S., 1998, Shale permeability characteristics; in *Current Research 1998-E*, Geological Survey of Canada, p. 183-192.

Keigwin, L.D., Rio, D., Acton, G.D., et al., 1998, Proc. ODP, Init. Repts., 172: College Station, TX (Ocean Drilling Program).

Kurihara, M., Sato, A., Funatsu, K., Ouchi, H., Yamamoto, K., Numasawa, M., Ebinuma, T., Narita, H., Masuda, Y., Dallimore, S.R., Wright, F., and Ashford, D., 2010, Analysis of Production Data for 2007/2008 Mallik Gas Hydrate Production Tests in Canada; International Oil and Gas Conference and Exhibition in China, 8-10 June 2010, Beijing, China.

Meyers, P.A., 1987, Appendix II. Organic carbon and calcium carbonate analysis, Deep Sea Drilling Project Leg 93, North American continental rise. *In* van Hinte, J. E., Wise, S. W, Jr., et al., Init. Repts. DSDP, 93, Pt. 2: Washington (U.S. Govt. Printing Office).

Milkov, A. V. and Sassen, R., 2001. Estimate of gas hydrate resources, northwestern Gulf of Mexico continental slope, *Marine Geology*, v. 179, p. 71-83.

Mountain, G.S., Miller, K.G., Blum, P., et al., 1994, Proc. ODP, Init. Repts., 150: College Station, TX (Ocean Drilling Program).

- Myers, R., 1978, Carbon-carbonate analysis, *In* Benson, W. E., Sheridan, R. E., et al., 1978. Initial Reports of the Deep Sea Drilling Project, v. 44: Washington (U.S. Government Printing Office), p. 983-986.
- Norris, R.D., Kroon, D., Klaus, A., et al., 1998, Proc. ODP, Init. Repts., 171B: College Station, TX (Ocean Drilling Program).
- Paull, C.K., Matsumoto, R., Wallace, P.J., et al., 1996, Proc. ODP, Init. Repts., 164: College Station, TX (Ocean Drilling Program).
- Paull, C.K., Matsumoto, R., Wallace, P.J., and Dillon, W.P. (Eds.), 2000. Proc. ODP, Sci. Results, 164: College Station, TX (Ocean Drilling Program). [doi:10.2973/odp.proc.sr.164.2000](https://doi.org/10.2973/odp.proc.sr.164.2000)
- Pickard, G.L., 1964, Descriptive Physical Oceanography: An Introduction, Macmillan, New York, 119 p.
- Poag, C. W., Watts, A. B., et al., 1987, Init. Repts. DSDP, 95: Washington (U.S. Govt. Printing Office).
- Price, P.B. and Sowers, T., 2004, Temperature dependence of metabolic rates for microbial growth, maintenance and survival: Proceedings of the National Academy of Sciences, v. 101, no. 13, p. 4631-4636 (March 30, 2004).
- Sassen, R., and Post, P. J., 2008, Enrichment of diamondoids and ¹³C in condensate from Hudson Canyon, US Atlantic, Organic Geochemistry, 39, p. 147–151.
- Shedd, W., Boswell, R., Frye, M., Godfriaux, P., and Kramer, K., 2011. Occurrence and nature of “bottom simulating reflectors” in the northern Gulf of Mexico, Marine and Petroleum Geology xxx, 1-10.
- Sheridan, R. E., Gradstein, F. M., et al., 1983, Init. Repts. DSDP, 76: Washington (U.S. Govt. Printing Office).
- Sloan, E.D., Jr., 1998, Clathrate hydrates of natural gases: Marcel Dekker, Inc., New York, 641 p.
- Spinelli, G. A., Gaimbalvo, E.R. and Fisher, A.T., 2004. Sediment permeability, distribution, and influence on fluxes in oceanic basement.
- Tucholke, B.E., Bryan, G.M., and Ewing, J.I., 1977, Gas-hydrate horizons detected in seismic-profiler data from the western North Atlantic, AAPG Bulletin, v. 61, No. 5, p. 698-707.
- White, S.M., 1979. Grain-size and carbon/carbonate analyses, holes 417, 418, Legs 51, 52, 53. *In* Donnelly, T., Francheteau, J., Bryan, W., Robinson, P., Flower, M., Salisbury, M., et al., Initial Reports of the Deep Sea Drilling Project, v. 51, 52, 53, Part 1: Washington (U.S. Government Printing Office), p. 715-718.

Appendix A. Atlantic setup parameter file run R31

Parameter	Type	Value1	Value2	Value3	Value4	Description
Study Name		R31				Title for this study
Input Data File Name		..Data\Att 2012_input.csv				Input Data Set pathname
Ntrials	Constant	1000				Number of trials (0 < Ntrials < 4000)
CellSize	Constant	9842.52				Linear size of cell (in feet)
SaveChargeCT	Constant	0				Save Charge Cell by Trial Output? (0=No,1=Yes)
SaveNetHSZCT	Constant	0				Save NetHSZ Cell by Trial Output (0=No,1=Yes)
SaveConcenCT	Constant	0				Save Concentration Cell by Trial Output (0=No,1=Yes)
SaveVolumeCT	Constant	0				Save Volume Cell by Trial Output (0=No,1=Yes)
SaveTechRecCT	Constant	0				Save Technically Recoverable Vol Cell by Trial Output (0=No,1=Yes)
GeoThermal Gradient	Beta	8.0583	5.2975	15	45	Geothermal Gradient beta(shape1,shape2),min,max
BottomTempCoeffs1	Constant	12.563	-0.0071054			WBT=wbtcoeff1*exp(wbtcoeff2*WD1)+wbtcoeff3+Error
BottomTempCoeffs2	Constant	1194	-0.78			
BottomTempCoeffs3	Constant	4.1				
BottomTempCutPts	Constant	1000	1444			
BottomTempError	Normal	0	0.62	0.0556	0.184	Error term in above (Note: only standard deviation is used)
Zeta	Normal	1.23	0.09			Local Salt -scale (mean, std dev)
Nu	Normal	0.03	0.003			Local Salt - shape (mean, std dev)
Mu	Normal	214	58.8			Hydrate stability temp - shift (mean, std dev)
Pi	Normal	0.11	0.01			Hydrate stability temp - scale (mean, std dev)
GammaA	Beta	14.405	0.298	31.365	10	Phase stability eqns, w/anomalies
DeltaA	Beta	0.298	14.405	7.689	10	Phase stability eqns, w/anomalies
GammaNo	Beta	1.0000	0.0101	40.284	5	Phase stability eqns, wo/anomalies
DeltaNo	Beta	0.0101	1.0000	8.233	1	Phase stability eqns, wo/anomalies
PlistMy	Gamma	1.638	1			Total Thickness of Sediment - Plisotocene (shape, scale)
PlioMy	Gamma	1.5	1			Total Thickness of Sediment - Pliocene (shape, scale)
UMMy	Gamma	0.976	1			Total Thickness of Sediment - Upper Miocene (shape, scale)
MMMy	Gamma	0.976	1			Total Thickness of Sediment - Middle Miocene (shape, scale)
LMMMy	Gamma	1.133	1			Total Thickness of Sediment - Lower Miocene (shape, scale)
SandPermCoeffs	Constant	10.85	-0.000258			Perm(md) =(Lambda* [a + b*Depth(m)) + Error] + 1)^(1/Lambda)
Lambda	Constant	0.153				Lambda in Sand Permeability Equation
SandPermError	Normal	0	2.541			Error term in above (Note: only standard deviation is used)
Omega	Normal	0.84	0.08			Shale porosity as fn of depth (mean, std dev)
Tau	Normal	-0.125	0.01			Shale porosity as fn of depth (mean, std dev)
Omicron	Normal	0.0037	0.00037			Shale permeability as fn of depth (mean, std dev)
Chi	Normal	1.7	0.17			Shale permeability as fn of depth (mean, std dev)
TOC	Weibull	1.1443	0.88536			Total Organic Carbon - Weibul (shape scale)
OmtQual	Weibull	1.6983	217.631			Asymptotic conversion efficiency (shape, scale)
MigRat	Constant	0	0			Fraction dip; set to 0; all vertical
SSFracVoid	Triangular	0	5	15		% Anomaly Fracture Void - Sand (min, most likely, max)
SHFracVoid	Triangular	0	5	15		% Anomaly Fracture Void - Shale (min, most likely, max)
SS1Coef	Constant	0.5583				ShallowSandPorosity = SS1Coef*exp(SS2Coef*Depth(m)) + Error
SS2Coef	Constant	-0.0008932				Shallow sand porosity (Note: must be negative)
SSPorError	Normal	0	0.05839			Error term in above (Note: only standard deviation is used)
SH1Coef	Constant	-0.71956				Shallow shale porosity (logit regression model)
SH2Coef	Constant	0.001756				Shallow shale porosity
SH3Coef	Constant	0				Shallow shale porosity
ShPorError	Normal	0	0.015			Shallow shale porosity error (Note: only standard deviation is used)
FracSat	Triangular	70	80	90		% saturation of fracture void volumes in anomalies only - sand/shale (min, most likely, max)
SandSat	Beta	5.6535	3.0424	0	100	% saturation matrix pore volumes - sand (shape1,shape2,min,max)
SHSat	Exponential	4	100			% saturation matrix pore volumes - shale (mean, max)
SedDensity	Constant	2.1				Sediment Density at Seafloor (in g/cc)
MigrationEff	Hard wired	0	0			Migration efficiency is fn of BSR = 0, 1 or 2 (see charge.f)
TrappingEff	Hard wired	1	0			Trapping Efficiency = 1
FormationVolFactor	Beta	5	1.6	139	33	Formation Volume Factor 139 < fvf < 172
SWD	Constant	23				% of cells which have strong water drive
SGR	Uniform	16	21			% Residual Gas Saturation
PA	Constant	1000				Pressure at abandonment (psi)
SGMA	Constant	0.55				Specific Gravity of Methane at abandonment
MaxInitProd	Lognormal	2.8842	1.2686	1000000		Maximum Initial Product

Notes: Rows shaded in gray are not used; those in red reflect changes to parameters; dummy (unused) variables must remain in as place holders.

Appendix B: Geothermal Gradient Workflow

Geothermal gradient (GTG) information is a requirement for the BOEM gas hydrate assessment model in order to calculate hydrate stability zone (HSZ) thickness and gas generation capacity. The multi-step approach presented here was used to develop a distribution of GTG values that were applied to the entire Atlantic Outer Continental Shelf (OCS).

First, we examined The Global Heat Flow Database of the International Heat Flow Commission (<http://www.heatflow.und.edu/data.html>), where the most recent data collection appears to be from 1986. Figure B-1 presents a map view and histogram of 99 heat flow (HF) datapoints that are within 200 nautical miles of the US Exclusive Economic Zone (EEZ) boundary. The mean HF = 43.5 milliwatts per square meter (mW/m^2). We assume that HF measurements (mW/m^2) approximately equal GTG ($^{\circ}C/km$) by adopting a nominal thermal conductivity of 1 watt per meter Kelvin ($W/(m-K)$).

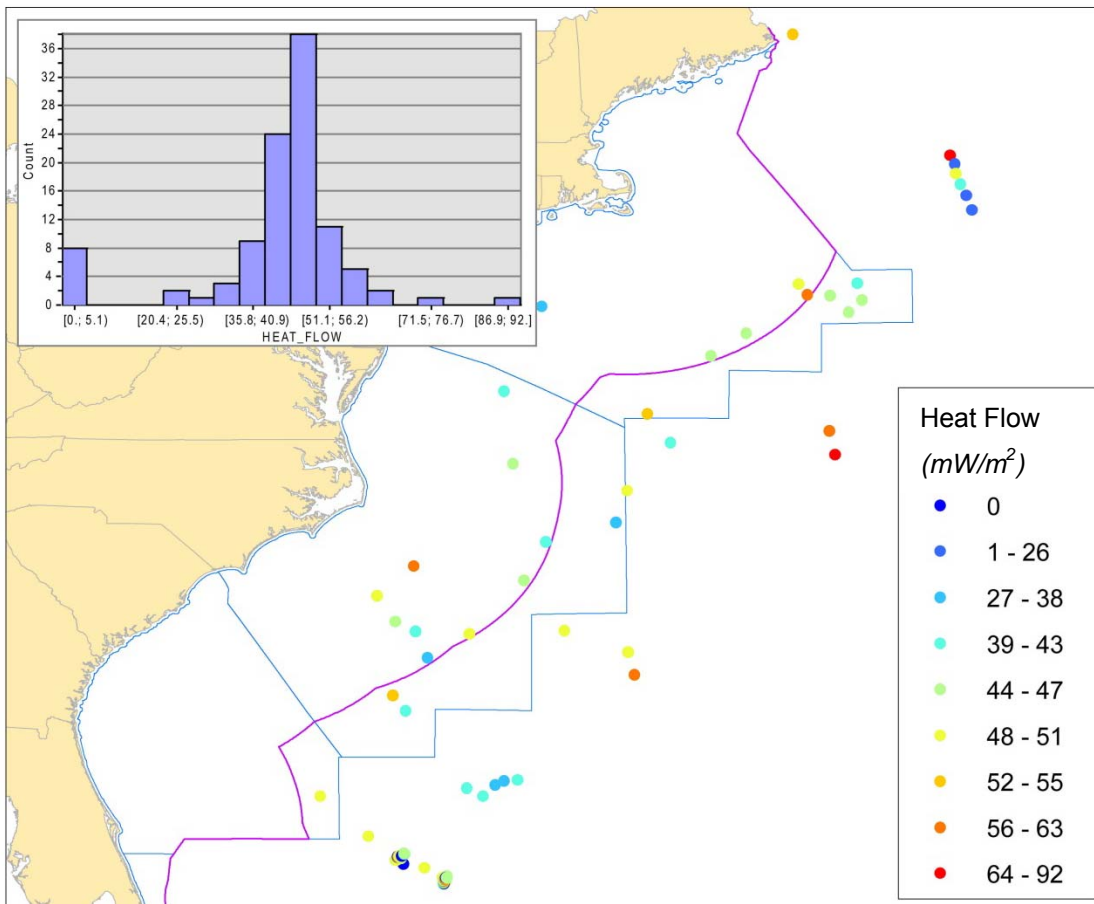


Figure B-1. Heat Flow measurements from the Global Heat Flow Database proximal to the United States coastline (units = mW/m^2). Mean value of the 99 data points shown here is $43.5 mW/m^2$. US EEZ line shown in purple.

Second, we examined 113 traditional measurements of heat flow from the Blake Ridge area of the southeastern U.S. (Ruppel et al, 1995), where mean HF $\sim 49 mW/m^2$ (excluding measurements directly above salt diapirs). Figure B-2 below shows map location of these measurements.

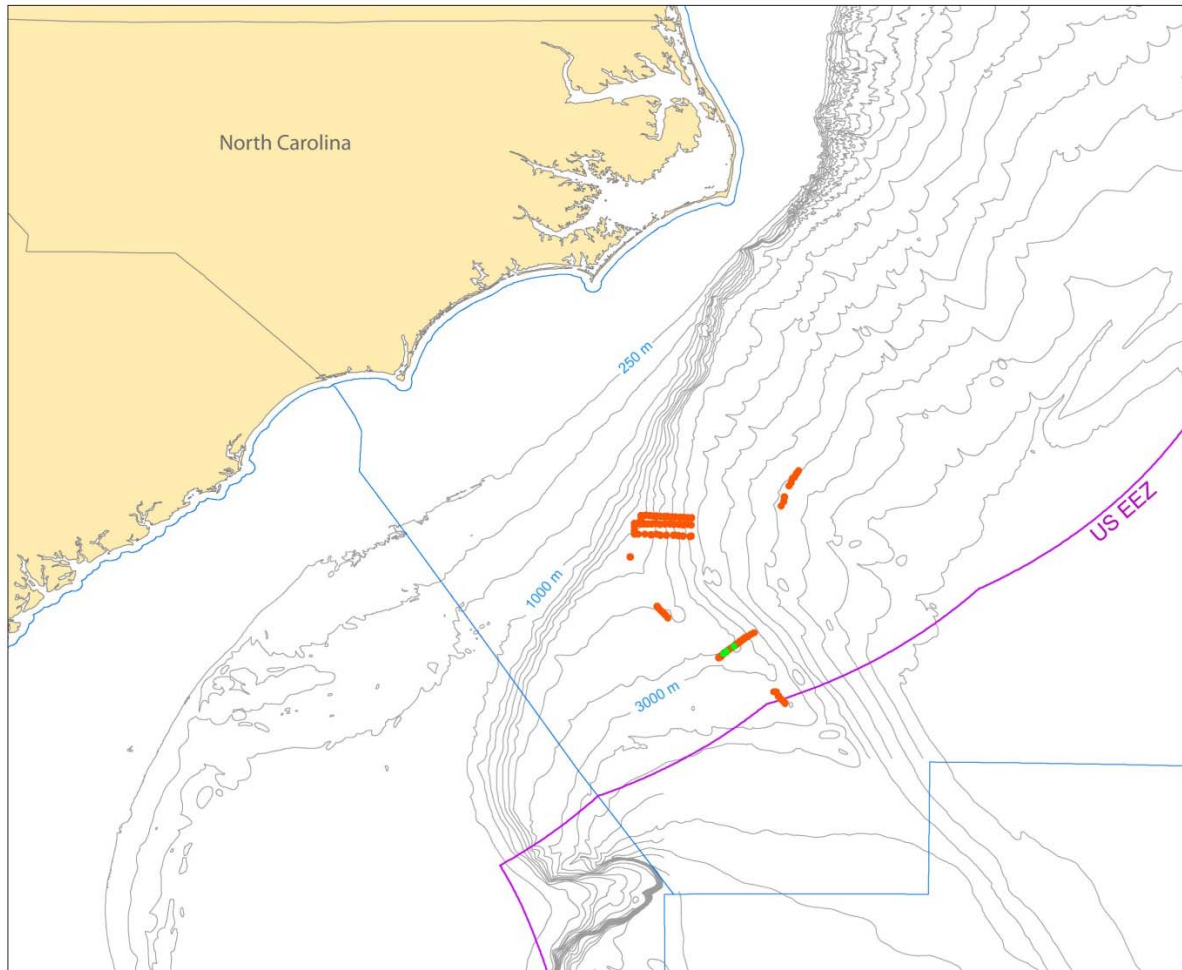


Figure B-2. Heat flow measurements ($n = 113$) from Ruppel et al (1995), shown as orange points on the map. ODP Leg 164 well sites 994, 995, and 997 are shown as green points. Bathymetric contour interval = 250 meters.

Third, we examined GTG information for three Ocean Drilling Program (ODP) Leg 164 sites on the Blake Ridge based on in situ temperature measurements of the formation (locations shown in Figure B-2). Ruppel (1997) reports the following gradient information based on sample depths that were within several hundred meters below the seafloor: Site 994 = $33.3\text{ }^{\circ}\text{C}/\text{km}$; Site 995 = $32.7\text{ }^{\circ}\text{C}/\text{km}$; and Site 997 = $36.9\text{ }^{\circ}\text{C}/\text{km}$.

Figure B-3 provides a map view comparison of the HF measurements from Ruppel et al (1995) and the formation temperature-derived GTG measurements (Ruppel, 1997) from the ODP Leg 164 sites 994 and 995 on the Blake Ridge (both shown as $^{\circ}\text{C}/\text{km}$ units). Figure B-3 highlights the fact that GTG measurements in the low 30's (from sites 994 and 995) are proximal to the HF measurements in the high 40's.

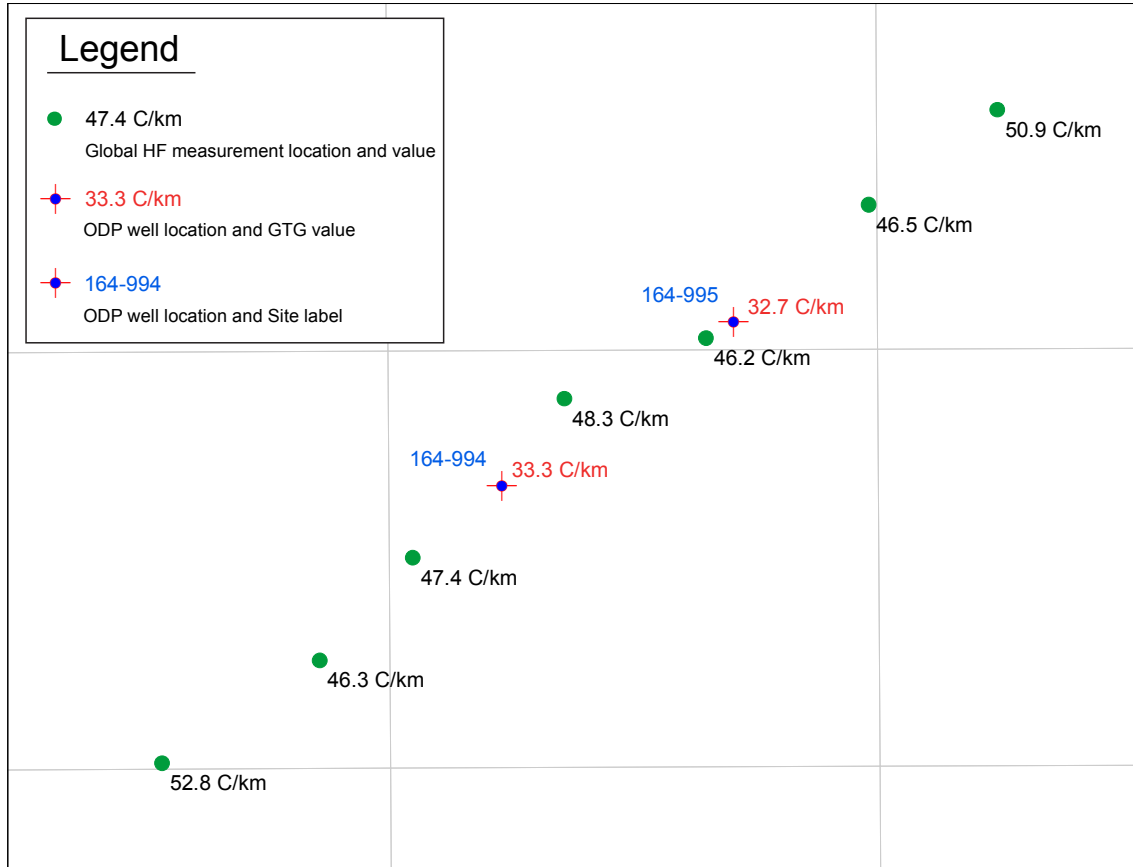


Figure B-3. Map view showing GTG and HF measurements from area of ODP Leg 164, sites 994 and 995 on the Blake Ridge. Gray lines are US OCS block boundaries (3 miles x 3 miles).

Based on the range of values obtained from these two measurement techniques, and the general deviation of the larger Global Heat Flow database (Figure B-1) from the three subsurface measurements of Ruppel (1997), we moved forward with an additional workflow, described below.

Geothermal Gradients from Bottom Simulating Reflectors

In our final approach to develop a GTG database for the Atlantic OCS, we modeled GTG using an approach similar to that described here:

From *Workshop on The Future of Marine Heat Flow: Defining Scientific Goals and Experimental Needs for the 21st Century*; 6-7 September 2007; Fort Douglas, University of Utah, UT; Co-conveners: R. N. Harris, A. T. Fisher, F. Martinez, and C. Ruppel: "...even without making heat flow measurements, the thermal regime in marine sediments can sometimes be estimated [e.g., Yamano *et al.*, 1982, Kaul *et al.*, 2000] when seismic data reveal a bottom simulating reflector (BSR),"

We are fortunate to have a fairly widespread distribution of very well defined BSRs in the Atlantic (see Figure 9, this report)¹⁵. To make the back-calculations necessary to arrive at GTG from BSR, the following workflow was employed:

¹⁵ Fundamentally, we assume that the seismic expression of the BSR is equivalent to the base of gas hydrate stability.

- Step 1:** On each 2-D line where BSR exists, map the water bottom (WB) and BSR;
- Step 2:** calculate thickness interval from WB to BSR (measured as an isochron using two-way travel time units (TWT));
- Step 3:** dump database of WB depth (TWT) and WB to BSR thickness (TWT) from each line interpretation at pre-determined spacing intervals (these points contain lat/long associations);
- Step 4:** convert TWT to depth (meters).

Water depth and depth to BSR at Leg 164 locations from Collett and Ladd (2000) are shown in Table B-1 below. Sediment velocity is obtained for time to depth conversion using the workflow described below.

Leg 164 Hole	MBSF to base HSZ (base logging unit 2)	Water Depth (meters)
994 D	428.8	2797.6
995 B	450.0	2774.6
997 B	450.9	2763.6

Table B-1. Depth to the top and bottom of the downhole log identified logging units in Holes 994D, 995B, and 997B.

Using a GIS query, we select all BSR points (from seismic interpretation) within 1000 meters of ODP Leg 164 wells 994, 995, and 997 (Figure B-4 and Tables B-2, B-3, and B-4). Apply depth to BSR to each of these TWT measurements to evaluate sediment velocity. Apply depth to WB to evaluate water velocity¹⁶.

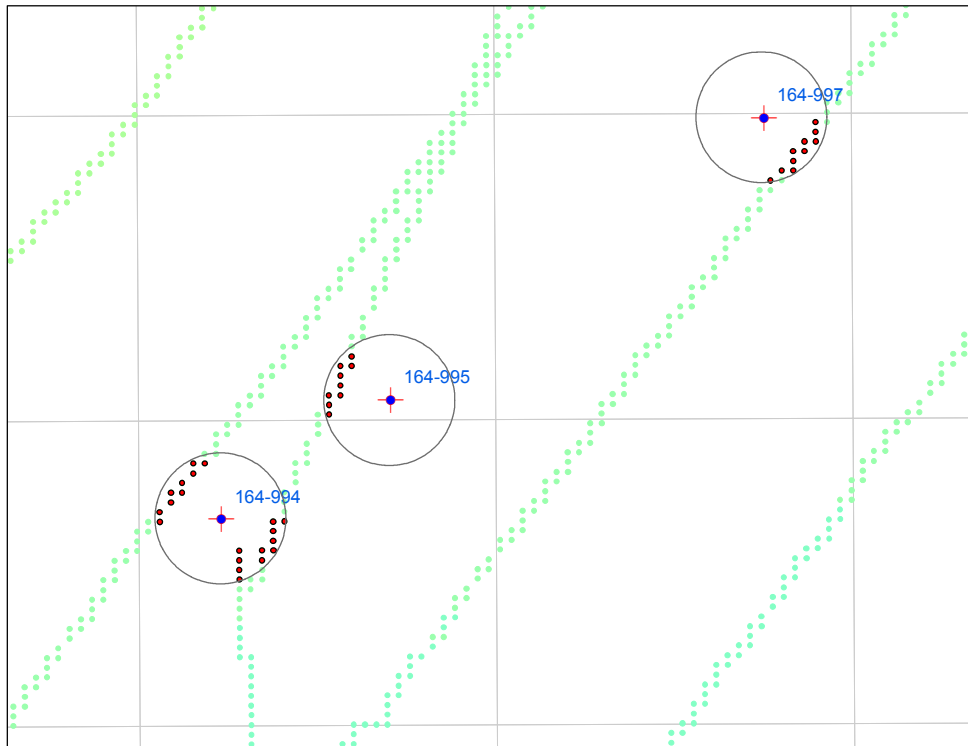


Figure B-4. GIS-queried seismic interpretation points within 1,000 meters of ODP Leg 164 sites 994, 995, and 997.

¹⁶ Formula: $thickness = (0.5)(isochron)(velocity)$

LONG	LAT	BSR_TIME (TWT)	BATHYMETRY (TWT)	BSR Isochron (TWT BSF)	Calc. sed velocity using 450.9 mbsf BSR (m/sec)	Calc. water velocity using 2763.6 m WD (m/sec)
-75.46806	31.83412	4260	3715	545	1654.68	1487.78
-75.46646	31.83550	4260	3715	545	1654.68	1487.78
-75.46486	31.83826	4261	3713	548	1645.62	1488.58
-75.46485	31.83688	4260	3713	547	1648.63	1488.58
-75.46485	31.83551	4260	3714	546	1651.65	1488.18
-75.46326	31.83964	4260	3712	548	1645.62	1488.98
-75.46325	31.83826	4259	3713	546	1651.65	1488.58
-75.46166	31.84240	4259	3713	546	1651.65	1488.58
-75.46165	31.84102	4260	3714	546	1651.65	1488.18
-75.46164	31.83965	4259	3714	545	1654.68	1488.18

Table B-2. Site 997 Query Results and Calculations.

LONG	LAT	BSR_TIME (TWT)	BATHYMETRY (TWT)	BSR Isochron (TWT BSF)	Calc. sed velocity using 450.0 mbsf BSR (m/sec)	Calc. water velocity using 2774.6 m WD (m/sec)
-75.5307	31.80363	4228	3697	531	1694.92	1501.00
-75.53069	31.80225	4229	3699	530	1698.11	1500.19
-75.53068	31.80088	4229	3700	529	1701.32	1499.78
-75.52911	31.80776	4222	3690	532	1691.73	1503.85
-75.52909	31.80501	4227	3693	534	1685.39	1502.63
-75.52909	31.80363	4228	3695	533	1688.56	1501.81
-75.52751	31.80914	4218	3687	531	1694.92	1505.07
-75.5275	31.80777	4221	3689	532	1691.73	1504.26

Table B-3. Site 995 Query Results and Calculations.

LONG	LAT	BSR_TIME (TWT)	BATHYMETRY (TWT)	BSR Isochron (TWT BSF)	Calc. sed velocity using 428.8 mbsf BSR (m/sec)	Calc. water velocity using 2797.6 m WD (m/sec)
-75.55475	31.78703	4251	3733	518	1655.60	1498.85
-75.55474	31.78565	4249	3735	514	1668.48	1498.05
-75.55315	31.78978	4239	3730	509	1684.87	1500.05
-75.55155	31.79116	4243	3727	516	1662.02	1501.26
-75.55154	31.78979	4240	3729	511	1678.28	1500.46
-75.54996	31.79392	4248	3721	527	1627.32	1503.68
-75.54835	31.79393	4245	3720	525	1633.52	1504.09
-75.54343	31.77883	4315	3759	556	1542.45	1488.48
-75.54342	31.77745	4315	3764	551	1556.44	1486.50
-75.54023	31.78159	4272	3745	527	1627.32	1494.05
-75.53864	31.78572	4263	3736	527	1627.32	1497.64
-75.53863	31.78297	4268	3742	526	1630.42	1495.24
-75.53862	31.78160	4269	3744	525	1633.52	1494.44
-75.53703	31.78573	4259	3734	525	1633.52	1498.45

Table B-4. Site 994 Query Results and Calculations.

From this GIS analysis, 32 datapoints were found to be within 1000 meters laterally of the three Leg 164 well locations. Site 997 yields 10 datapoints, Site 995 yields 8, and Site 994 yields 14, as shown in Tables B-2 through B-4 above. Two datapoints from the 994 site were found to be anomalous and were removed. The remaining 30 datapoints are compiled in a single table (Table B-5) and yield an average sediment velocity of 1660 m/sec (range 1627 to 1701 m/sec), and an average water velocity of 1496 m/sec (range 1488 to 1505 m/sec).

Site	LONGITUDE	LATITUDE	BSR_TIME (tw)	BATHYMETRY (tw)	ISOPACH (tw)	VEL_CALC (m/sec)	Vel_water (m/sec)
997	-75.46326	31.83964	4260	3712	548	1645.62	1488.98
997	-75.46325	31.83826	4259	3713	546	1651.65	1488.58
997	-75.46166	31.8424	4259	3713	546	1651.65	1488.58
997	-75.46485	31.83688	4260	3713	547	1648.63	1488.58
997	-75.46486	31.83826	4261	3713	548	1645.62	1488.58
997	-75.46164	31.83965	4259	3714	545	1654.68	1488.18
997	-75.46485	31.83551	4260	3714	546	1651.65	1488.18
997	-75.46165	31.84102	4260	3714	546	1651.65	1488.18
997	-75.46806	31.83412	4260	3715	545	1654.68	1487.78
997	-75.46646	31.8355	4260	3715	545	1654.68	1487.78
995	-75.52751	31.80914	4218	3687	531	1694.92	1505.07
995	-75.5275	31.80777	4221	3689	532	1691.73	1504.26
995	-75.52911	31.80776	4222	3690	532	1691.73	1503.85
995	-75.52909	31.80501	4227	3693	534	1685.39	1502.63
995	-75.52909	31.80363	4228	3695	533	1688.56	1501.81
995	-75.5307	31.80363	4228	3697	531	1694.92	1501.00
995	-75.53069	31.80225	4229	3699	530	1698.11	1500.19
995	-75.53068	31.80088	4229	3700	529	1701.32	1499.78
994	-75.54835	31.79393	4245	3720	525	1633.52	1504.09
994	-75.54996	31.79392	4248	3721	527	1627.32	1503.68
994	-75.55155	31.79116	4243	3727	516	1662.02	1501.26
994	-75.55154	31.78979	4240	3729	511	1678.28	1500.46
994	-75.55315	31.78978	4239	3730	509	1684.87	1500.05
994	-75.55475	31.78703	4251	3733	518	1655.60	1498.85
994	-75.53703	31.78573	4259	3734	525	1633.52	1498.45
994	-75.55474	31.78565	4249	3735	514	1668.48	1498.05
994	-75.53864	31.78572	4263	3736	527	1627.32	1497.64
994	-75.53863	31.78297	4268	3742	526	1630.42	1495.24
994	-75.53862	31.78160	4269	3744	525	1633.52	1494.44
994	-75.54023	31.78159	4272	3745	527	1627.32	1494.05

Table B-5. *Thirty measurements used to calculate average velocities.*

The average velocities (1496 m/sec and 1660 m/sec) were then applied to original seismic measurements to convert from two way travel time to water bottom depth and sub-seafloor depth (BSR).

With this database in hand, we calculated at each location of seismic data BSR interpretation, the GTG necessary to satisfy the gas hydrate phase stability relationship.

The computations for GTG were performed on data sets comprising 50,695 observations. Each observation consists of a longitude, latitude, base of gas hydrate stability (meters; referred to in this report as HSZ¹⁷), and water depth (WD) in meters.

The estimates were made using the R functions `GTG.fn` and water bottom temperature function `wbt.fn`.

```
GTG.fn<-function(HSZ,WD){
  GTG<-1000*(-wbt.fn(WD)+8.9*log(HSZ+WD)-50.1 - 1.5)/HSZ
  return(GTG)}
```

The above function results from setting $f(HSZ|WD) = 0$ and solving iteratively for GTG

$$f(HSZ | WD) = -[GTG \times \frac{HSZ}{1000}] - WBT + [\delta \times \ln(HSZ + WD) - \gamma] - \lambda.$$

The above equation expressed in math form is:

$$GTG = 1000 \times (-WBT + [\delta \times \ln(HSZ + WD) - \gamma] - \lambda) / HSZ.$$

The $\lambda = 1.5$ reflects the ambient salinity of 35; there is no influence of local salt. For purposes of establishing the GTG distribution, delta (δ) = 8.9 and gamma (γ) = 50.1, the fitted values from Milkov and Sassen (2001) corresponding to CH₄ = 100%.

Results

The data file was modified to include only 47,379 of the original 50,695 points, as the initial calculation yields some anomalously high GTG measurements (> 60 °C/km) that, after further review on seismic data, prove to be erroneous picks at the seismic data level. Many of the anomalously warm GTG values coincided with areas of the seafloor that exhibit channels or incisions, or were found to be proximal to areas of shallow salt. For the purpose of this study - to provide an empirical data set of GTG values that can be broadly applied across the Atlantic OCS - we retain only those GTG values that appear to represent ambient conditions.

Figure B-5 presents a map view of the final data points that were calculated for this study. A histogram of these data is presented in Figure B-6. The mean GTG value of 33.16 °C/km from our computed database is in very close agreement to those GTG values measured by Ruppel (1997) on the Blake Ridge. We have not included any seafloor heat flow measurements in our final distribution, as we determine that these are consistently reporting higher thermal conditions which cannot be rectified with the widespread geophysical data observations.

¹⁷ HSZ refers to the thickness of section between the seafloor and the base of gas hydrate stability, rather than explicit areas that may or may not allow for the formation of gas hydrate. We recognize that gas hydrate will likely not be stable in the upper part of the HSZ, and that gas hydrate may also be stable within the water column.

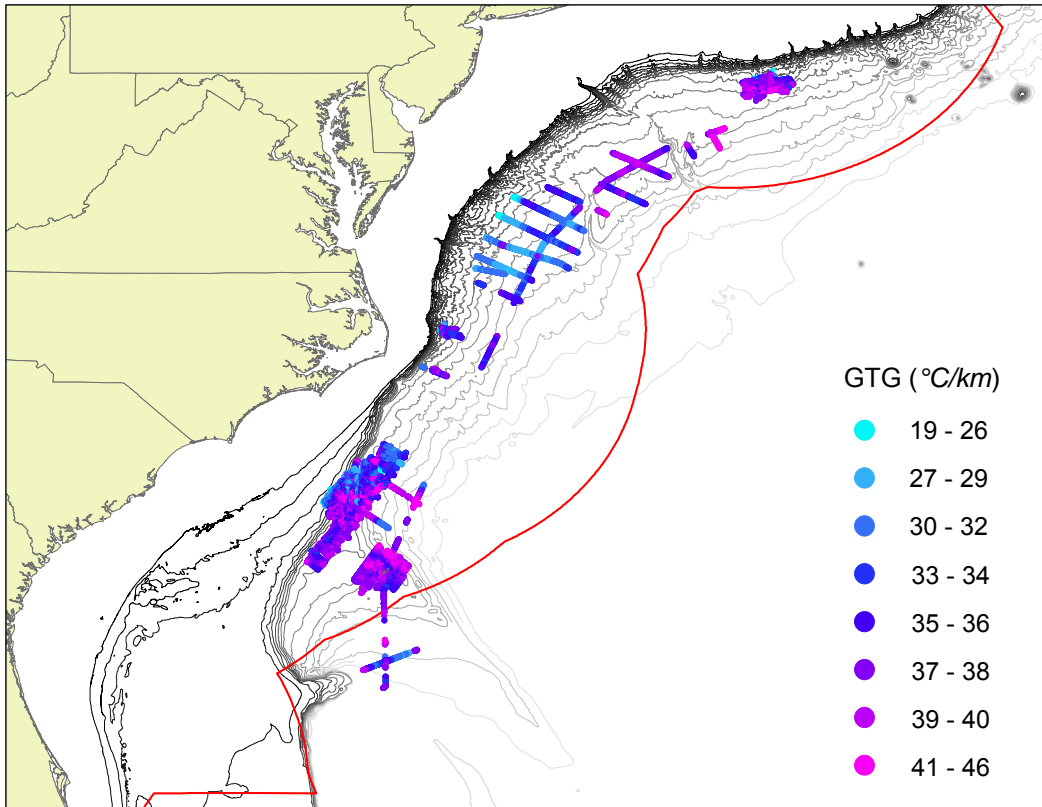


Figure B-5. Location of seismic data interpretations used to calculate GTG. Values are expressed as °C/km.

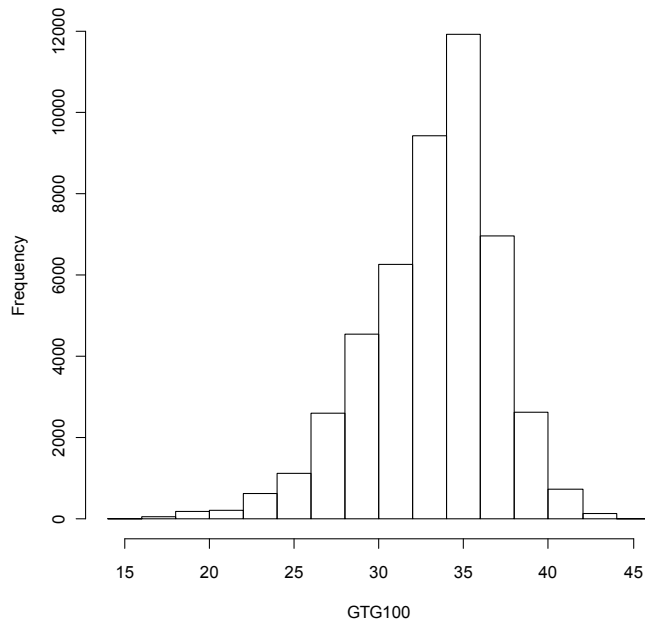


Figure B-6. Histogram of calculated GTG measurements for the Atlantic OCS. ($n = 47,379$; mean = 33.16 °C/km). Figure also shown as Figure 28 in main body of report.

References – Appendix B

Harris, R.N., A. T. Fisher, F. Martinez, and C. Ruppel, 2007, *Workshop on The Future of Marine Heat Flow: Defining Scientific Goals and Experimental Needs for the 21st Century*; 6-7 September 2007; Fort Douglas, University of Utah, UT.

Kaul, N., A. Rosenberger, and H. Villinger, 2000, Comparison of measured and BSR-derived heat flow values, Makran accretionary prism, Pakistan, *Mar. Geol.*, 164, 37–51.

Ruppel, C., R.P. Von Herzen, and A. Bonneville, 1995, Heat flux through an old (~175 Ma) passive margin: offshore southeastern USA, *Journal of Geophysical Research*, 100,, 20,037-20,058.

Ruppel, C., Anomalously cold temperatures observed at the base of the gas hydrate stability zone, 1997, U.S. Atlantic passive margin, *Geology*, 25, 699-702.

Yamano, M., S. Uyeda, Y. Aoki, and T.H. Shipley, 1982, Estimates of heat flow derived from gas hydrates, *Geology*, 10, 339–343.

Appendix C. Shallow Shale Porosity Model

The Hamilton (1976) shallow shale porosity model is replaced with a logit function of porosity that both keeps porosity between 0 and 1 and represents porosity as monotone decreasing with increasing depth. To this end define

$$\begin{aligned} d &= \text{Depth below seafloor (meters)} \\ P(d) &= \text{Porosity as a function of depth} \end{aligned}$$

and set

$$P(d) = \frac{1}{1 + \exp\{a + b \times d\}} \quad (1)$$

Then

$$\ln \left[\frac{1 - P(d)}{P(d)} \right] = a + b \times d \quad (2)$$

If we append an error term to Hamilton's model, it is of the form

$$P_H(d) = \beta_0 + \beta_1 \times d + \beta_2 \times d^2 + \varepsilon, \quad (3)$$

which is a regression model with residual error ε indexed by parameters β_0 , β_1 , β_2 , and

$\sigma^2 = \text{Var}(\varepsilon)$. In the computations shown below we assume that $\text{Var}(\varepsilon) = 0.015^2$.

In the absence of porosity versus depth data, we can identify reasonable values of logit parameters a and b by matching the mean of Hamilton's model and the logit model (2) at two arbitrary depths, 100 meters and 1000 meters. Thus, we set

$$\frac{1}{1 + \exp\{a + b \times 100\}} = \beta_0 + \beta_1 \times 100 + \beta_2 \times 100^2 = \kappa_1$$

$$\frac{1}{1 + \exp\{a + b \times 1000\}} = \beta_0 + \beta_1 \times 1000 + \beta_2 \times 1000^2 = \kappa_2$$

As κ_1 and κ_2 are known numbers (Table 8 of main report), we can, for a coherent pair κ_1, κ_2 , solve for a and b . By coherent, we mean a pair of shale porosity values that both lay between 0 and 1 and for which porosity at the shallower depth is greater than that at greater depth.

This pair of equations can be recast as a pair of linear equations which can then be solved for a and b :

$$\ln\left(\frac{1 - \kappa_1}{\kappa_1}\right) = a + b \times 100 \quad \text{and} \quad \ln\left(\frac{1 - \kappa_2}{\kappa_2}\right) = a + b \times 1000. \quad (4)$$

At 100 meters, (3) yields a mean porosity of 0.633 and at 1000 meters mean porosity is 0.260. We solve

$$-0.543 = a + b \times 100 \text{ and } 1.046 = a + b \times 1000$$

and find $a = -0.71956$ and $b = 0.001756$. Now replace Hamilton's equation with:

$$P(d) = \frac{1}{1 + \exp\{-0.71956 + 0.001756 \times d\}} \quad (5)$$

Matching Residual Error Variances

The logit model (2) implies that porosity is a function of depth d and, in addition, of the random error ε . Define

$$P(d, \varepsilon) = \frac{1}{1 + \exp\{a + b \times d + \varepsilon\}}.$$

Then the variance of porosity is

$$Var(P(d, \varepsilon)) = Var\left(\frac{1}{1 + \exp\{a + b \times d + \varepsilon\}}\right), \quad (6)$$

a nonlinear function of the random variable ε . To get a first order approximation to (6) at a given depth d , compute a Taylor series expansion of (6) in ε with ε in a neighborhood of zero:

$$Var(P(d, \varepsilon)) = Var(P(d, 0) + P'(d, 0) \times \varepsilon + O(\varepsilon^2)) \cong [P'(d, 0)]^2 \times Var(\varepsilon) \quad (7)$$

provided that terms in ε^q , $q > 1$ converge (in mean square) to zero. Here we assume that an approximation of the form (7) is reasonable, as

$$P'(d, 0) = -\frac{\exp\{a + b \times d\}}{[1 + \exp\{a + b \times d\}]^2} = -P(d, 0) \times [1 - P(d, 0)]. \quad (8)$$

A first order approximation to the variance of porosity represented as

$$Var(P(d, \varepsilon)) \cong [P'(d, 0)]^2 \times Var(\varepsilon) = [P(d, 0)(1 - P(d, 0))]^2 \times Var(\varepsilon). \quad (9)$$

From (7)

$$P(d) \cong P(d, 0) = \frac{1}{1 + \exp\{-0.71956 + 0.001756 \times d\}}.$$

To match the variance regression residual error assigned to Hamilton's quadratic regression for porosity as a function of depth, 0.015^2 choose a depth d and set

$$\frac{0.015}{P(d, 0) \times (1 - P(d, 0))} = Std Dev(\varepsilon). \quad (10)$$

Appendix D: Case Study - Blake Ridge area near ODP wells 994, 995, 997

Ocean Drilling Program (ODP) Leg 164 was the first dedicated effort to investigate gas hydrate accumulations in the marine environment (Paull et al, 2000). Drilling efforts in Leg 164 were focused on an anomalous geophysical feature on the Blake Outer Ridge (Figure D-1) that was interpreted as a bottom simulating reflector (BSR) indicative of gas hydrate presence. Significant vertical accumulations (> 200 m) of gas hydrate were recorded in three wells (Sites 994, 995, and 997) drilled during Leg 164.

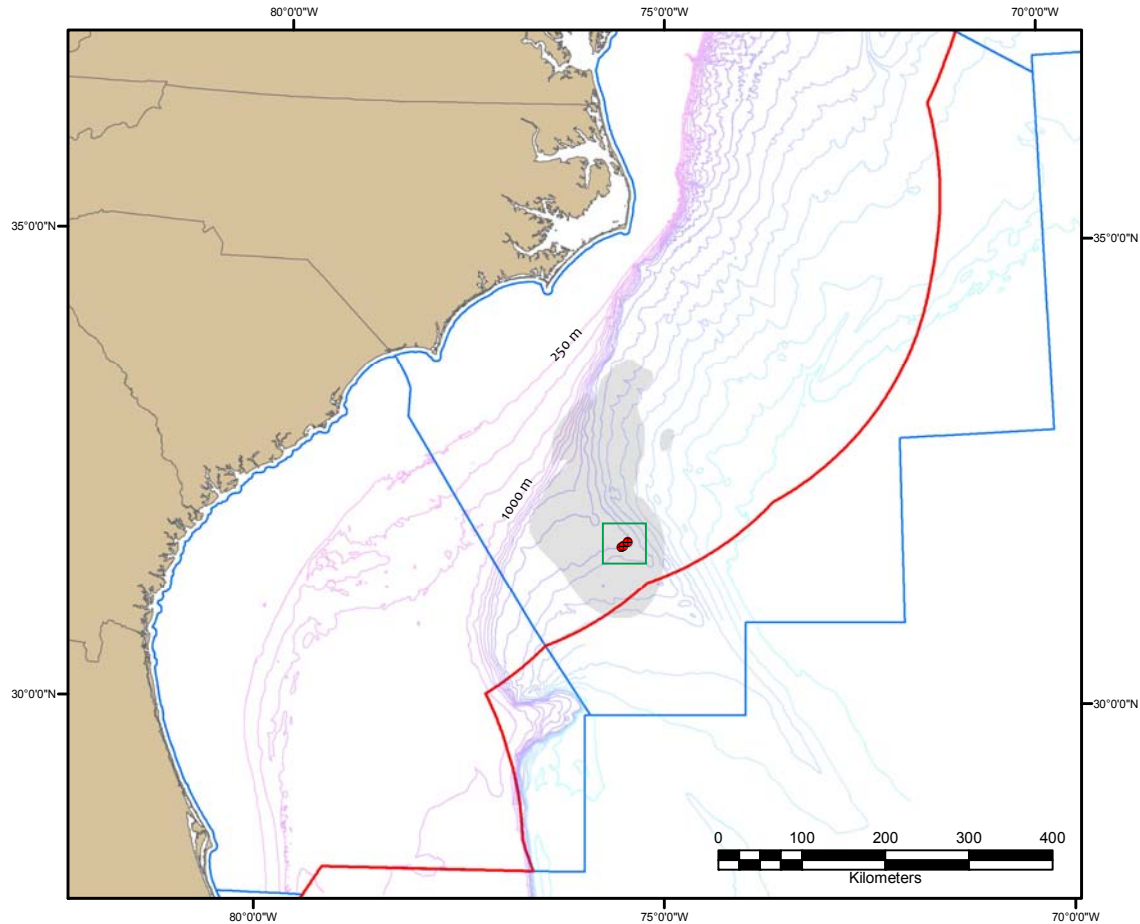


Figure D-1. Location map for ODP Leg 164 site 994, 995, and 997 wells used in calibration effort. Area inside green box is enlarged in Figure D-2. Contours are water depth ($CI = 250$ m). Shaded grey area is interpreted extent of the Blake Ridge BSR.

Collett and Ladd (2000) provided a volumetric assessment of in-place gas hydrate on the Blake Ridge through interpretations of well log and borehole data extrapolated over the area coincident with the BSR. Interpreted volumes and unit volumes are shown in Table D-1 below (modified from Collett and Ladd, 2000).

Site	Depth of logging Unit 2 (mbsf)	Thickness of hydrate-bearing zone (m)	Sediment porosity (%)	Gas-hydrate saturation (%)	Volume of hydrate/km ² (m ³)	Volume of gas within hydrate/km ² (m ³)
994	212.0-428.8	216.8	57.0	3.3	4,083,577	669,970,673
995	193.0-450.0	257.0	58.0	5.2	7,731,352	1,267,941,673
997	186.4-450.9	264.5	58.1	5.8	8,839,915	1,449,746,073

Table D-1. *Interpreted wellbore results from ODP 164 locations Site 994, 995, and 997 and volumetric estimates of gas hydrate density proximal to well locations (modified from Collett and Ladd, 2000).*

BOEM gas hydrate resource assessment volumes have been calibrated to calculated gas hydrate volumes on the Blake Ridge presented by Collett and Ladd (2000). The map presented in Figure D-2 shows our assessment results in the immediate vicinity of the ODP well locations 994, 995, and 997 in units similar to those presented in the table above (units on Figure D-2 are *billion m³/km²*). Note that the mean results from this study (and shown in Figure D-2 below) are much more uniform than, and do not display the variability of, those results shown in Collett and Ladd (2000). Large variations in BOEM model inputs are not realized in a presentation of mean results from the BOEM model. BOEM model results align closely with the interpreted volumes at Site 994 (and less so with Sites 995 and 997) largely because of the mean gas hydrate saturation value that we assign to shale-dominated reservoirs.

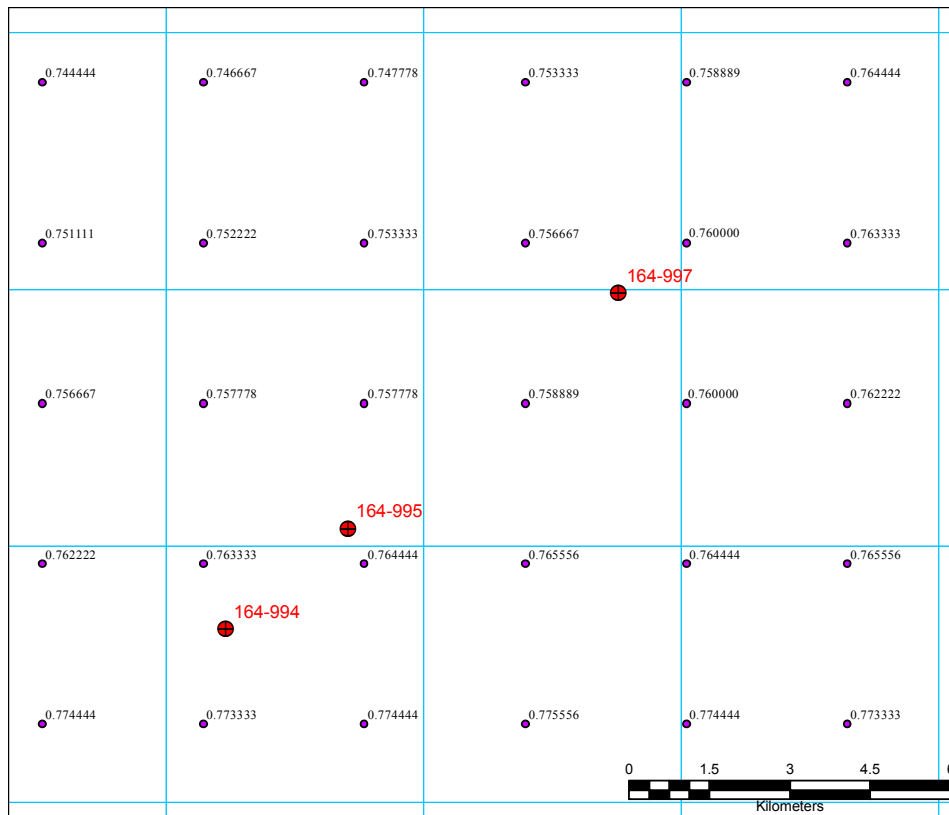


Figure D-2. *In-place gas hydrate volume on the Blake Ridge around ODP Leg 164 Sites 994, 995, and 997. Purple dots represent the center of a BOEM model cell; labels are the BOEM model mean in-place gas hydrate volume for that cell, expressed as billion m³ / km². Light blue squares are 3 mile x 3 mile OCS lease blocks.*